

**CLIMBING RIPPLE SUCCESSIONS IN TURBIDITE SYSTEMS:
DEPOSITIONAL ENVIRONMENTS, SEDIMENTATION RATES, AND
ACCUMULATION TIMES**

Zane R. Jobe^{1*}, Donald R. Lowe¹, William R. Morris²

1. Department of Geological and Environmental Sciences, Stanford University, 450 Serra Mall, Building 320, Stanford, CA, 94305, USA
2. ConocoPhillips, Houston, TX 77079, USA

Email: Zane R. Jobe zanejobe@gmail.com
 Donald R. Lowe drlowe@stanford.edu
 William R. Morris william.r.morris@conocophillips.com

ABSTRACT

Climbing-ripple cross-lamination (CRCL) is most commonly deposited by turbidity currents when suspended load fallout and bedload transport occur contemporaneously. The angle of ripple climb reflects the ratio of suspended load fallout and bedload sedimentation rates, allowing for the calculation of the flow properties and durations of turbidity currents. Three areas exhibiting thick (> 50 m) sections of deep-water CRCL deposits are the focus of this study: 1) the Miocene upper Mount Messenger Formation in the Taranaki basin, New Zealand, 2) the Permian Skoorsteenbergh Formation in the Tanqua depocenter of the Karoo basin, South Africa, and 3) the lower Pleistocene Magnolia Field in the Titan basin, Gulf of Mexico. Facies distributions and local

contextual information indicate that CRCL in each area was deposited in an ‘off-axis’ setting where flows were expanding due to loss of confinement or a decrease in slope gradient. The resultant reduction in flow thickness, Reynolds number, shear stress, and capacity promoted suspension fallout and thus CRCL formation. CRCL in the New Zealand study area was deposited both outside of and within channels at an inferred break in slope, where flows were decelerating and expanding. In the South Africa study area, CRCL was deposited due to a loss of flow confinement. In the Magnolia study area, an abrupt decrease in gradient near a basin sill caused flow deceleration and CRCL deposition in off-axis settings. Sedimentation rate and accumulation time were calculated for 44 CRCL sedimentation units from the three areas using TDURE, a mathematical model developed by Baas et al. (2000). For T_c divisions and T_{bc} beds averaging 26 and 37 cm thick, respectively, average CRCL and whole bed sedimentation rates were 0.15 and 0.26 mm/s and average accumulation times were 27 and 35 minutes, respectively. In some instances, distinct stratigraphic trends of sedimentation rate give insight into the evolution of the depositional environment.

CRCL in the three study areas is developed in very fine- to fine-grained sand, suggesting a grain size dependence on turbidite CRCL formation. Indeed, the calculated sedimentation rates correlate well with the rate of sedimentation due to hindered settling of very fine- and fine-grained sand-water suspensions at concentrations of up to 20% and 2.5%, respectively. For coarser grains, hindered settling rates at all concentrations are much too high to form CRCL, resulting in the formation of massive/structureless S_3 or T_a divisions.

1. INTRODUCTION

Climbing-ripple (CR) bedforms and climbing-ripple cross-lamination (CRCL) were first recognized and described by H.C. Sorby over 150 years ago (Sorby, 1852, 1859). As predicted by Sorby (1859), CRCL has proved to be a useful sedimentary structure for calculating sediment accumulation rates (Bucher, 1919; Reineck, 1961; Jopling and Walker, 1968; Allen, 1970, 1971a, 1971b) and identifying the environment and conditions of deposition (Walker, 1967; Mutti, 1977; Rubin and Hunter, 1982). CRs are common in fine-grained turbidite systems (e.g., Kuenen, 1953; Bouma, 1962; Kuenen, 1967; Walker, 1969; Mutti and Normark, 1987; Hodgson et al., 2006; Luthi et al., 2006), likely because non-uniform turbidity currents deposit sediment from suspension concurrently while passing through the ripple stability field (Allen and Leeder, 1980; Baas, 2004; Sumner et al., 2008).

Despite all the research conducted on CRCL, no study has focused on determination of the specific depositional settings of deep-water CRCL and on estimating flow properties of turbidity currents based on the physical characteristics of CRCL deposits. This study focuses on three areas where CRCL is especially abundant and widely distributed: 1) the Miocene upper Mount Messenger Formation in the Taranaki basin, New Zealand, 2) the Permian Skoorsteenberg Formation in the Tanqua depocenter of the Karoo basin, South Africa, and 3) the lower Pleistocene Magnolia Field reservoir, Gulf of Mexico. This study explores the geometry and distribution of CRCL in these areas, the environmental settings within which it formed, and the characteristics of the depositing flows.

2. CLIMBING RIPPLES

2.1. How and Why Current Ripples Climb

Current ripples are developed most commonly in very-fine- to fine-grained sand (Stanley, 1974; Southard and Boguchwal, 1990) and represent bedload transport by a lower-flow-regime unidirectional current (Raudkivi, 1963). Figure 1 shows the general morphology and terminology of current ripples. Boundary layer separation at the ripple crest and reattachment at the reattachment point (Fig. 1; Raudkivi, 1963) create a downstream-propagating asymmetric bedform that has a characteristic height H (5-30 mm) and wavelength λ (10-30 cm) (Leeder, 1999). The ripple index, defined as λ/H (Tanner, 1967), usually ranges from 5 to 40 (Tanner, 1967; Leeder, 1999) and is somewhat dependent on plan view morphology (Allen, 1963).

Climbing ripples require not only bedload transport but also concurrent rapid suspended load fallout rates (Sorby, 1859). When suspended sediment falls rapidly onto a bed with active bedload transport within the ripple-stability field, erosion at the reattachment point may be reduced or suppressed completely, resulting in incomplete removal of ripples as they migrate. Consequently, upstream ripples climb over the next downstream ripple (Fig. 2). The angle of climb reflects the interplay of suspended-load fallout rate and bedload transport rate according to:

$$\tan\zeta = \frac{RH}{2j_b} \quad (1)$$

where ζ is the angle of climb, R is the suspended-load fallout rate, H is the observed ripple height, and j_b is the bedload transport rate (Allen, 1970).

2.2. Areas of CRCL Formation

Climbing ripples require lower flow regime bedload transport *and* high rates of suspended load fallout. These conditions are most commonly associated with non-uniform flows where decreasing turbulence intensity over relatively short distances results in an abrupt loss of capacity (Hiscott, 1994; Kneller, 1995) and consequently rapid suspended load fallout. Turbulence intensity can be measured by the flow Reynolds number (Reynolds, 1883):

$$Re = \frac{v\rho_f L}{\mu} \quad (2)$$

where v is velocity of the flow, ρ_f is the fluid density, L is the flow depth, and μ is the fluid viscosity. Non-uniformity in turbidity currents is usually associated with a rapid decrease in v , commonly caused by a break in slope, or a reduction in L , commonly associated with a loss of confinement. Decreasing v and/or L acts to lower Reynolds number, decreasing local turbulence intensity and increasing suspended-load fallout rate for flows transporting at capacity. Hence, in deepwater settings, CRCL is most commonly developed: **1**) on levees and along channel-margins (McKee, 1966; Mutti, 1977; Morris et al., 2000) where flow stripping (*sensu* Piper and Normark, 1983; Fildani et al., 2006) is common; **2**) at channel mouths (Mutti and Normark, 1987; Wynn et al., 2002) and associated lobe and splay settings (Walker, 1967), where confinement is lost; and **3**) in areas where slope gradient abruptly decreases (Bursik and Woods, 2000; Maier et al., 2011), such as at the base-of-slope (Mutti and Normark, 1987). Rapid gradient changes are especially common in topographically complex basin settings, including active-margin and salt-influenced basins (e.g., Prather et al., 1998; Clark and Cartwright, 2009; Jobe et al., 2010; Maier et al., 2011). In addition, local topographic complexity

(e.g. Adeogba et al., 2005; Armitage et al., 2009) may drive flow non-uniformity and thus CRCL deposition.

2.3. Classification of CRCL Deposits

Plan-view morphology, cross-sectional geometry, and the angle of climb are common metrics by which CR and CRCL are classified (e.g., Walker, 1963; Jopling and Walker, 1968; Allen, 1973; Harms, et al., 1975). With time, ripple plan-view morphology evolves from simple, straight-crested forms to equilibrium linguoid forms (Baas, 1994, 1999). The time required to reach equilibrium depends on the shear stress (i.e. flow velocity), and equilibrium ripple forms are always linguoid (Baas, 1994, 1999). Thus, the plan-view ripple morphology can be qualitatively related to flow conditions and durations.

Hunter (1977) divided climbing ripples into two categories based on their cross-sectional geometry and climb angle: subcritical and supercritical (Fig. 2; Hunter, 1977), terms not to be confused with identical terms describing flow stage according to the Froude number. The critical angle of climb is that in which “the vector of ripple climb is parallel to the steepest part of the ripple stoss slope” (Hunter, 1977). Consequently, subcritical CRCLs, also termed type A by Allen (1973), have low climb angles ($\sim 0\text{-}15^\circ$) and partial stoss side erosion. Supercritical CRCLs, termed type B by Allen (1973), display high climb angles ($\sim 15\text{-}45^\circ$) and stoss side preservation (Fig. 2). CRCLs that have very steep angles of climb and more symmetric cross-sections are termed sinusoidal lamination, or type S (Allen, 1973); these are essentially aggrading bedforms with climb angles in excess of 45° (Fig. 2) that exhibit no significant downstream ripple migration.

Sinusoidal lamination has been considered to indicate very high rates of suspension fallout in a waning current (Allen, 1963; Jopling and Walker, 1968; Hunter, 1977). Subcritical CRCL, supercritical CRCL, and sinusoidal lamination describe climb angle and the resultant cross-sectional geometry and can occur for any ripple plan-view morphology.

3. GEOLOGIC SETTING OF CRCL LOCALES IN THIS STUDY

The three locales (Fig. 3) that are the focus of this study were chosen due to the striking CRCL successions in each. These CRCL successions are thick, both in terms of the entire succession, generally > 50 m, and the thickness of individual sedimentation units, commonly > 1 m. These locales will be abbreviated as (Fig. 3): Miocene upper Mount Messenger Formation, New Zealand (**NZ**); Permian Skoorsteenberg Formation, Tanqua depocenter, Karoo basin, South Africa (**ZA**); and Pleistocene Magnolia Field, deep-water Gulf of Mexico (**MAG**).

3.1. Upper Mount Messenger Formation, Taranaki Basin, New Zealand (NZ)

The Taranaki basin exists mainly offshore of the west coast of the north island of New Zealand (Fig. 3A), but basin sediments outcrop locally on beach cliffs and are inferred to continue inland, where outcrops are sparse due to extensive vegetation. The basin has a complex tectonic history, with many episodes of extension and shortening related to subduction along the east coast of the north island of New Zealand (King and Thrasher 1992, 1996; King, 2000). During the late Miocene, the Taranaki basin was in a back-arc position and subsiding, providing a deep-marine environment for the deposition

of the Mount Messenger Formation (Fig. 3F). Generally, the local source area was to the south, resulting in north-northwestward sediment transport (King et al., 1993). Highly variable in terms of facies, the lower Mount Messenger includes thick-bedded sandy turbidites, mass transport deposits, and burrowed silty turbidites (King et al., 1993, 1994; Browne et al., 2000). The upper Mount Messenger is a > 100 m thick, very fine-grained sandstone-mudstone succession that has intervals of CRCL-rich deposits; it is well exposed in coastal cliffs at Pukearuhue beach (Fig. 3F inset). Browne and Slatt (2002) interpreted this succession as a channel-levee complex on a base-of-slope apron.

3.2. Skoorsteenbergr Formation, Tanqua Karoo, South Africa (ZA)

The Tanqua depocenter in the Western Cape province of South Africa (Fig. 3B) includes a well-studied Permian deep-water sedimentary succession developed in the Karoo retro-arc foreland basin (Fildani et al., 2007). The Upper Permian Skoorsteenbergr Formation consists of six discrete sandstone packages interpreted as stacked submarine fan systems separated by mudstone units (Wickens, 1994; Morris et al., 2000; Hodgson et al., 2006). ‘Fan 3’ (Fig. 3D), the best exposed and most studied (e.g., Wickens and Bouma, 2000; Morris et al., 2000; Johnson et al., 2001a; van der Werff and Johnson 2003; Hodgson et al., 2006; Luthi et al., 2006; Prelat et al., 2009), consists of very fine- to fine-grained sandstone representing both channel and lobe depositional settings (Morris et al., 2000). CRCL deposits occur in the non-channelized areas of Fan 3 (Morris et al., 2000), such as the Kleine Reit Fontein locale (Fig. 3D), the focus of this study. Flows moving into the basin from the west-southwest show an abrupt deflection to the north in eastern outcrops (Fig. 3D), interpreted to result from the presence of a

tectonically-induced topographic buttress along the eastern margin of the basin (Hodgson et al., 2006; Luthi et al., 2006).

3.3. Magnolia Field, Gulf of Mexico (MAG)

The Magnolia Field, a producing oil and gas field operated by ConocoPhillips, is located at the southern edge of the Titan mini-basin in the Gulf of Mexico (Figs. 3C, E) in 1,433 m water depth and with reservoir depths of ~3700 m below mudline (Weissenburger and Borbas, 2004). The southward filling of the basin (Fig. 3E) evolved through ponded, transitional, and bypass phases (*sensu* Prather et al., 1998; Weissenburger and Borbas, 2004). The main reservoir of lower Pleistocene age occupies the transitional phase of basin fill (Haddad et al., 2003). This reservoir has been interpreted by Haddad et al (2003) and McGee et al. (2003) as an off-stacking, erosionally-confined channel complex. Seismic and borehole data indicate that the reservoir is heterogeneous and includes thick, blocky sandy turbidites, mass transport deposits, and thinner bedded CRCL-rich successions. Furthermore, fluid pressure, phase, and compositional data indicate that the reservoir is highly segmented and compartmentalized (Weissenburger and Borbas, 2004; McCarthy et al., 2005, 2006) due to syn-and post-depositional faulting due to allochthonous salt movement. The only cored well in the field, located near the salt-cored sill of the mini-basin (Fig. 3E), contains 61 m of thick- and thin-bedded, very-fine-grained sand and silty deposits rich in CRCL.

4. CRCL FACIES

Classifying CRCL deposits using their physical geometries/morphologies and stacking patterns (i.e., facies) is useful for qualitative analysis of flow conditions at, as well as boundary conditions of, the site of deposition. Using the morphology and stacking patterns of the CRCL deposits from NZ, ZA, and MAG, four facies are termed Facies 1, 2, 3, and 4 (Figs. 4A-D and Figs. 5-8, respectively). These facies do not represent different flow types, but rather a *modified* Bouma sequence that reflects the downslope evolution of flow properties due to changes in boundary conditions (Fig. 9) or the relative magnitude of the flow. All sand-bed grain sizes are very fine- to fine-grained sand (Table 1).

4.1. Facies 1: Long-Lived and/or Rapidly Depositing Surging Flows

Description: Facies 1 units are the thickest sedimentation units observed in this study, up to 2.2 m thick (Figs. 4A, 5). Basal contacts are generally flat but sometimes erosive; upper contacts preserve ripple topography. Facies 1 units are composed of high velocity plane-laminated divisions alternating with CRCL (Figs. 4A, 5). Beds generally begin with a basal plane-laminated layer and subsequently show alternating CRCL divisions and plane-laminated divisions. The uppermost CRCL division generally shows CRCL with an upward-increasing angle of climb (Fig. 4A, 5).

Interpretation: Due to plane-laminated T_b divisions and common basal erosion, Facies 1 flows were the most vigorous of any facies and likely represent the highest observed shear stresses and Reynolds numbers. However, these flat laminations are thickened (Fig. 5), probably a result of concurrent suspension fallout (cf. Bridge, 1997). This suggests that the rate of deposition may have been quite high. The alternation of T_b

and T_c CRCL divisions indicate that flows evolved through multiple surges with fluctuating suspension fallout rates before finally depositing the capping CRCL division with an increasing angle of climb. The thick-bedded nature and surging of Facies 1 units suggests that the depositing flows were relatively long-lived and/or rapidly depositing.

4.2. Facies 2: Collapsing Flows

Description: Facies 2 units are spectacular single sedimentation events with an increasing angle of climb throughout the bed (Fig. 4B, 6). These units consist of subcritical CRCL overlain by supercritical CRCL overlain by sinusoidal lamination (Figs. 4B, 6). No other sedimentary structures underlie or overlie the CRCL in Facies 2 units, except in NZ, where thin T_b divisions are sometimes present at the base (Fig. 6A). Basal contacts are non-erosional and average bed thickness is approximately 1 m (Fig. 7). Upper bed contacts often preserve ripple topography (Fig. 6).

Interpretation: The thick-bedded nature, predictive succession of CRCL, and absence of erosion in Facies 2 units suggests that flows were collapsing. The increasing angle of climb implies that suspension fallout rates were increasing throughout deposition relative to the bedload transport rate. Several Facies 2 deposits display abrupt changes in the angle of climb (Fig. 6B) that may indicate sudden flow collapse, while a shallowing then steepening climb angle (Fig. 6C) may indicate surging during flow collapse.

4.3. Facies 3: Intermediate, Waning Flows

Description: Facies 3 consists of medium-bedded CRCL sandstone interbedded with thin-bedded mudstone (Figs. 4C, 7). Bed thickness is variable between 15 cm and

50 cm (Fig. 7; Table 1), and sandstones consist entirely of CRCL (Fig. 7). Basal contacts are generally flat and begin with subcritical CRCL (Figs. 4C, 7). Typical successions include subcritical to supercritical CRCL with an increasing angle of climb, but lacking an upper sinusoidal laminated division (Figs. 7A, 7B), or beds consisting entirely of subcritical CRCL (Fig. 7C). Ripple topography is variably preserved (Figs. 4C, 7).

Interpretation: The incomplete succession of CRCL divisions and predominance of subcritical CRCL in Facies 3 suggests that flows had lower suspension fallout rates and/or shorter durations compared with flows that deposited Facies 1 and 2. The absence of sinusoidal lamination suggests that suspension fallout rates never reached extreme values.

4.4. Facies 4: Distal, Slow-Moving, Small-Volume Flows

Description: Facies 4 consists of thin-bedded CRCL sandstone interbedded with thin-bedded mudstone (Figs. 4D, 8). Sand bed thickness averages 3 cm, but is variable from 1 cm to 15 cm (Fig. 8). Original ripple topography is generally preserved and overlying beds do not erode or modify this topography (Figs. 4D, 8), resulting in a ‘pinch and swell’ bed geometry. Climb angles are generally less than 5° (Fig. 8). If sufficient mudstone deposition has healed the CR topography, the next sandstone bed has a flat base and a rippled top (see arrow in Fig. 8B), re-initiating the pinch and swell topography.

Interpretation: The low angle of climb and thin-bedded nature of Facies 4 indicate that relatively little suspended load fallout occurred during deposition relative to other

CRCL facies. The generally thin-bedded character also suggests that flows were thin, slow-moving, and volumetrically diminutive at the site of deposition.

4.5. Downslope and Head-to-Tail Evolution of CRCL-Depositing Turbidity

Currents

It is clear that in virtually all cases CRCL is deposited by non-uniform flows where the velocity (v) and flow depth (L) spatially vary. These changes are expressed in high suspended-load fallout rates, leading to CRCL. Turbidity currents commonly become non-uniform and depositional where they encounter abrupt decreases in slope, leading to a change in v ; where they move from a confined to a less confined setting, resulting in a decrease in v and/or L ; or where they experience a hydraulic jump, resulting in a decrease in v but increase in L . Flows responding to changes that produce non-uniformity are likely to experience a rapid drop in capacity (cf. Hiscott, 1994) and thus high-suspended load fallout rates. Downslope, such flows are likely to gradually re-equilibrate through deposition and velocity changes to local conditions and the suspended load fallout rate will decline. As a result, the deposits are likely to display a regular downslope series of structures (Fig. 9), reflecting initially the abrupt onset of non-uniformity and, subsequently, their gradual downslope re-equilibration. Immediately downflow from the initiation of non-uniform conditions, the initially high flow velocities and initially high suspended-load fallout rates should result in deposition of Facies 1 (Fig. 9). Farther downslope, a transition to Facies 2 is expected (Fig. 9) as suspended-load fallout rates reach maximum values and flow velocities rapidly decline. Suspended load fallout rates will be high compared to bedload transport rates because the flows lose

capacity. Facies 3 is expected further downslope (Fig. 9) as the flows begin to re-equilibrate, suspended load fallout rates decline, and suspended-load transport approaches capacity. Facies 4 is expected in the most distal environments (Fig. 9) and probably records the full re-equilibration of the currents and slow deposition related to gradually changing conditions of slope and flow thickness out into the basin.

Indeed this facies progression is seen in the ZA locale, where Facies 4 is much more common in distal areas (Hodgson et al., 2006; Jobe et al., 2008; also see section 5.2). In areas where turbidity currents are robust, such as a channel mouth, CRCL may be developed only in lateral and/or off-axis settings (Fig. 9) where flow is weak, allowing for bedform development (cf. Wynn et al., 2002). The above discussion assumes flows begin with constant volume. However, in an environment with a distribution of flow volumes, the presence of Facies 1-4 may also indicate relative flow magnitude and suspended sediment concentration. While large-volume flows may deposit all four facies during downslope evolution, small-volume flows may only be able to deposit lower energy facies.

4.6. CRCL Facies Proportions in the Three Study Areas NZ, ZA, and MAG

Figure 10 shows original and normalized percentage distributions of Facies 1-4 in the three study areas. Facies 1 is greatest in NZ at 37%, indicating that flows were generally more robust and contained periods of upper-flow regime T_b deposition. Contrastingly, Facies 1 makes up only 7% and 13% of the ZA and MAG locales (Fig. 10), indicating that most CRCL-depositing flows were not able to maintain sufficient shear stress to deposit T_b divisions or that they were not upper flow regime flows when

they became non-uniform. Facies 2 makes up 43% and 32% of the ZA and MAG locales (Fig. 10), indicating that flows were collapsing and exhibited high suspension fallout rates. Facies 2 comprises only 15% of the NZ locale, suggesting that many flows were not completely collapsing at the site of deposition; this inference is supported by the overwhelming quantity of Facies 1 in NZ. Facies 3 constitutes 13, 19, and 26% of the NZ, ZA, and MAG locales (Fig. 10); these similar proportions indicate that there were some flows in all locales that were waning, but suspension fallout rates or flow durations were not high or long enough to generate a complete Facies 2 CRCL unit. All areas have similar proportions of Facies 4 at about 30% (Fig. 10), suggesting that between large-volume events, many small-volume, slow-moving currents were active, similar to many other turbidite systems (e.g., Amy and Talling, 2006).

5. DESCRIPTIONS AND DEPOSITIONAL ENVIRONMENT

INTERPRETATIONS OF CRCL LOCALES

5.1. NZ (New Zealand) Locale

5.1.1. Description

Immediately north of the Waikaramarama River mouth (Fig. 3F), 14 beds in a 50 m CRCL-rich interval were studied to determine the rate and duration of sedimentation; these measurements have the designation NZ-N (Table 1). Higher stratigraphically and south of the Waikaramarama River, a stratigraphic section was measured through 60 m of CRCL-rich deposits (Figs. 11A, B), and 17 beds were studied, with the designation NZ-M (Table 1). A third locale, where 5 more beds with the designation NZ-S (Table 1)

were studied, lies stratigraphically above and to the south of NZ-M, with a covered and faulted interval separating the two sub-locales.

CRs in the NZ locale consist of non-equilibrium sinuous forms (Fig. 11D). Facies 1 makes up more than one-third of the NZ CRCL deposits (Figs. 10, 11A), with bed thickness averaging 62 cm. Facies 2 and 3 are less abundant (Fig. 10) and average bed thickness is 30 cm. Facies 4 is common in thin-bedded intervals (Fig. 11). Bioturbated mudstone units also make up a significant portion of the measured section (Figs. 11A, F), generally found above large truncation surfaces (Figs. 11A, B, E). These mudstones can be so thoroughly bioturbated as to destroy primary fabric and completely disarticulate thin sand beds (Fig. 11F). Paleoflow is generally to the north (Fig. 11A), although with considerable divergence.

5.1.2. Depositional setting interpretation

The thick-bedded CRCL units at Pukearuhue Beach were classified by Browne and Slatt (2002) as ‘proximal levee’ deposits on a ‘base-of-slope apron’. Indeed, some of the CRCL deposits occur outside of the channel (Fig. 11B), but many also pinch out against truncation surfaces (Fig. 11B), indicating intra-channel deposition. The high proportion of Facies 1 (Fig. 10) and the intra-channel CRCL deposition indicate that the NZ locale was relatively closer to the axis of flow than either the ZA or MAG locales. The non-amalgamated CRCL-rich facies (Figs. 11A, B, E) may be off-axis channel fill and overbank facies associated with a large submarine channel system, which are commonly observed in base-of-slope environments and channel-lobe-transition-zones (Wynn et al., 2002). Axial facies may also be CRCL, or may be higher energy facies,

such as the shell-hash and mud-clast conglomerate seen in lower stratigraphic intervals (Plate 49 of King et al., 1993).

Browne and Slatt (2002) inferred a break in slope (i.e., gradient change) for the NZ locale, and the wide variation in paleocurrent direction throughout the succession (Fig. 11A) supports this inference. This break in slope probably acted in three ways to promote CRCL deposition in the NZ locale: 1) the decrease in gradient would cause reductions in flow velocity and shear stress, thus increasing suspended-load fallout rates; and 2) an increase in channel width at the base-of-slope, as commonly documented in modern systems (Adeogba et al., 2005; Maier et al., 2011), can cause flow expansion and a reduction in flow thickness, resulting in flow non-uniformity and rapid suspended load fallout; and 3) a decrease in channel depth, also commonly observed in areas of decreasing gradient (Wynn et al., 2002), promotes flow thickness reductions and non-uniformity. The wide variation in paleocurrent directions throughout the succession (Fig. 11A; Browne and Slatt, 2002) supports the notion of flow non-uniformity and expansion at the inferred break in slope (Fig. 9).

5.2. ZA (South Africa) Locale

5.2.1. Description

Fan 3 outcrops have been extensively subdivided (Johnson et al., 2001a; van der Werff and Johnson, 2003; Hodgson et al., 2006), but only three main intervals are recognized by this study: lower and upper sand-prone packages separated by a mud-prone package (Fig. 12), all of which contain abundant CRCL. Due to exposure constraints (see Hodgson et al., 2006, p. 29-30), this study focuses on the lower sand-rich unit (Fig.

12D). More than 900 paleocurrent indicators were measured in this unit near Kleine Reit Fontein, yielding an overall average of $050^{\circ} \pm 10^{\circ}$ (Fig. 12A). CRs in the ZA locale consist of equilibrium and near-equilibrium linguoid forms (Fig. 12B). Facies 4 is present in the lower unit, but becomes increasingly more common in more distal outcrops to the north (Fig. 12). Facies 2 and 3 are abundant (Figs. 10, 12D), and Facies 1 occurs only when infilling small-scale concave-up truncation features (Figs. 12C, D). These truncation features are rare in western outcrops and relatively small, averaging 10 m wide and ~ 1 m deep (Figs. 12C, D), but increase in size and frequency to the east, averaging 30 m wide by 5 m deep in eastern outcrops (Fig. 12D); 21 measurements of truncation depths show a linear eastward increase in depth of 1 m per 400 m distance ($R^2 = 0.58$). Further to the east near Ongeluks River (Fig. 12A), morphologically similar but much larger erosional features are filled with massive/structureless sandstone (Fig. 12D; Morris et al., 2000; Hodgson et al., 2006). This eastward facies transition is poorly exposed between sections 13 and 4 (Fig. 12A).

5.2.2. *Depositional setting interpretation*

The facies distributions, stratal patterns, and relative location in the system indicate that the Kleine Reit Fontein area represents an off-axis environment that received unconfined flows. The predominance of Facies 2 and 3 in ZA (Fig. 10) indicates that the flows were highly depletive. The small-scale concave-up features are interpreted as scours (sensu Normark et al., 1979; Mutti and Normark, 1987) by this study and have similar geometries to ‘megaflutes’ (Elliott, 2000; Pyles, 2008; Kane et al., 2009). These scours are interpreted to represent robust, high shear-stress portions of flows that eroded

the bed, thereafter depositing Facies 1 in the newly created depressions. These features are thought to be temporary and infilled rather quickly, perhaps by no more than a few flows (e.g., Fig. 12C). The large-scale erosional features filled with structureless sandstone at Ongeluk River (Fig. 12D) are interpreted as erosionally confined thalwegs or channels (Morris et al., 2000; Hodgson et al., 2006) that reflect full flow confinement. The eastward transition from the CRCL-dominated Kleine Reit Fontein to the axial channelized Ongeluk River, a distance of approximately 2 km (Fig. 12A, D), likely reflects the influence of increasing confinement, shear stress, and particle concentration, with scour intensity steadily increasing eastward (Fig. 12D).

Paleocurrent data and regional mapping show that turbidity currents were sourced from the southwest, but abruptly turn northward just east of Kleine Reit Fontein (Figs. 4D, 12A; Hodgson et al., 2006). Also, Fan 3 thins rapidly east of wellbore NS4 (Fig. 4D; Hodgson et al., 2006, Luthi et al., 2006). These architectural changes are interpreted by Hodgson et al. (2006) and Luthi et al. (2006) to reflect the presence of tectonically-induced intra-basinal seafloor topography. This buttress may have acted to deflect flows northward and compress and re-invigorate them, causing the eastward increase in confinement and scour intensity observed in the off-axis Kleine Reit Fontein (Fig. 12D). In Ongeluk River outcrops near the topographic buttress, the flows may have 'bulked up' enough to form high-density turbidity currents (cf. Lowe, 1982), causing channel or thalweg incision. The tectonically-induced buttress, if growing during deposition, may account for the substantial thickness of CRCL deposits seen in the Kleine Reit Fontein area.

5.3. MAG (Magnolia Field, GOM) Locale

5.3.1. Description

The Magnolia field occurs adjacent to the southern salt-cored margin and exit point of the Titan mini-basin (Figs. 3E, 13A, B). A dip-oriented seismic reflection profile down the axis of the basin (Fig. 13C) reveals a ~70 m thick main reservoir interval thinning and partially onlapping onto the salt wall. A strike-oriented seismic reflection profile near the southern basin margin (Fig. 13D) shows chaotic high- and low-amplitude reflections and multiple truncation surfaces in the main reservoir interval. Well logs in the cored 2ST2 well show that the main reservoir package is composed of non-amalgamated sandstone-mudstone facies (Fig. 13C) while the same package in the A7 well is much thicker (240 m) and composed of thick, amalgamated sandstone (Fig. 13D; Haddad et al., 2003). However, seismic resolution is poor and amplitudes are generally not well correlated with lithology, so the differentiation of facies and architecture solely with seismic data is difficult. Pervasive slumping and faulting of the main reservoir interval in updip locations (Fig. 13B) adds additional complexity; thus, biostratigraphy was relied upon for inter-well correlation (Haddad et al., 2003).

The 2ST2 cored well is located in the updip part of the field (Figs. 13B, C), where heterolithic and chaotic seismic facies are common. The 61 m thick cored interval consists of CRCL sandstone interbedded with mudstone (Fig. 13E). Facies 2 and 3 are prevalent (Fig. 10), but beds are generally thinner than in NZ and ZA (Fig. 13F). Facies 4, with preserved ripple topography being common (Fig. 13F), makes up about a quarter of the CRCL interval (Fig. 10). However, a significant portion of the core (Fig. 10) consists of syn- to post-depositionally modified beds (Fig. 13E), including strata with

convoluted lamination (Fig. 13G) and slumped and extensively faulted intervals (Fig. 13H). Mud-clast lined scours are also evident in core (Fig. 13I) and dipmeter data (Kane et al., in press), many of which are similar in depth and facies to the ZA locale.

5.3.2. Depositional setting interpretation

The main Magnolia reservoir package has been interpreted by Haddad et al (2003) and McGee et al. (2003) to represent erosionally-confined channel complexes deposited by south-flowing turbidity currents. However, poor seismic imaging and faulting make individual channel differentiation problematic (Fig. 13D). Furthermore, the scours observed in the core (Fig. 13I) and dipmeter data further complicate channel differentiation and indicate that most incisions were not large-scale. At least one small, ~400 m wide channel/scour is associated with the amalgamated, 240 m thick sandstone package in the A7 well (Fig. 13D), but these small features cannot account for the thickness of the aggradational, seemingly ponded facies.

The transitional phase of mini-basin evolution during which the main reservoir package was deposited is just as commonly characterized by ponded facies as channelized, bypass facies (Prather et al., 1998). Rapid deposition and ponding in mini-basins, such as that seen in MAG, is commonly associated with an abrupt decrease in gradient as flows encounter a basin margin or sill (Lamb et al., 2006). The proximity of the salt-cored Titan mini-basin sill to Magnolia suggests that flows encountered a gradient change at the sill and rapidly decelerated and spread out, resulting in massive sandstone deposition in axial (e.g., A7 well) locales and CRCL-rich sandstone in off-axis (e.g., 2ST2 well) locales. The spatial relationship of the two wells (Fig. 13B) suggests

that axial south flowing turbidity currents near the A7 well may have supplied the off-axis 2ST2 environment upon gradient-inspired flow divergence. Any flows that reached the basin sill likely continued down-system, but probably would have had greatly reduced suspended-load sediment concentrations. The thickness of the CRCL-dominated package (Fig. 13E) suggests that these topographic conditions were maintained despite continued deposition, perhaps by syn-depositional allochthonous salt movement. The extensive slumping and faulting present in updip locations (Figs. 13G, H) are consistent with syn- and post-depositional deformation.

5.4. Summary

Each locale studied shows different depositional architecture, local topographic irregularities, and facies proportions useful for determination of the depositional environment, relative slope gradient, level of confinement, and relative position of the axis of flow. Figure 14 shows each locale diagrammatically in order to demonstrate controls on CRCL formation. In NZ, the CRCL was deposited both outside of and within channels (Fig. 14A). An abrupt decrease in regional gradient at the base of slope (Fig. 14A) may have caused flows to decelerate and deposit CRCL.

Flows in the ZA locale were likely sourced from an axial thread of flow, perhaps a large channel, located to the southwest of Kleine Reit Fontein (Fig. 14B). Flow tops stripped from flows within this channel (*sensu* Piper and Normark, 1983) would have experienced an abrupt reduction in flow thickness, promoting CRCL deposition (Fig. 14B). However, as flows progressed to the northeast, they encountered the basin-margin

topographic buttress (Fig. 14B) that acted to focus flow, causing a shift in flow direction, scouring, and eventual channelization (Fig. 14B).

The complex mini-basin topography present in the MAG locale is a prime environment for CRCL formation. The large gradient decrease associated with the basin sill likely caused ponding, producing massive sands in axial locales (A7 well) and CRCL-rich facies in off-axis locales (cored 2ST2 well). The divergence of flows associated with this break in slope probably created widespread flow expansion and non-uniformity, resulting in off-axis CRCL deposition and small scouring (Fig. 14C). Analogous to ZA, an increase in scour intensity may be expected closer to the MAG sill as flows were compressed and focused by the sill topography (Fig. 14C). Robust flows may have been able to top the sill and continue down-system (Fig. 14C).

This study shows that CRCL may develop in a variety of deep-water environments where flows experience non-uniformity caused by flow thickness reductions due to channel mouth unconfinement or flow stripping, or by abrupt decreases in gradient, commonly associated with the base of slope or a basin margin (Fig. 14). When associated with scours, as in the ZA and MAG locales, flow thickness reductions may be attributed to hydraulic jumps or cyclic steps (e.g., Fildani et al., 2006). Decreased flow thickness results in flow expansion and/or deceleration, thus decreasing Reynolds number and shear stress. The resultant flow is less turbulent and therefore has less capacity (*sensu* Hiscott, 1994), promoting suspended-load fallout and thus CRCL formation. If these topographic conditions are maintained through allogenic processes such as allochthonous salt growth or tectonically induced buttress growth, favorable flow

conditions can be sustained for protracted time intervals, forming major thicknesses of CRCL-rich deposits such as those seen in the three studied locales.

6. FLOW PROPERTY ESTIMATION USING CRCL DEPOSITS FROM THE THREE LOCALES

6.1. Estimating Flow Properties Using CRCL

A rigorous analysis of water-laid CRs and CRCL was undertaken by J.R.L. Allen during the early 1970s. Using the sediment transport theory of Bagnold (1966), Allen (1970, 1971a) developed methods to estimate flow velocity, bedload transport rate, suspension fallout rate, and accumulation time of CRCL deposits using relationships between the CRCL ripple height, climb angle, and grain size. Allen (1971a) validated this theoretical reasoning with flume experiments and also applied it to the interpretation of outcropping CRCL deposits. The sedimentation rate at the transition between a high-velocity plane-laminated division (T_b) and a climbing-rippled division (T_c) was given by Allen (1971a, 1971b, 1991) as:

$$R_{bc} = 9.386 \frac{D_{bc}^{1.5} \tan \xi}{H_{bc}} \quad (3)$$

where R_{bc} (Fig. 15) is the sedimentation rate in m/s at the T_{bc} boundary, 9.386 is a SI-unit appropriate coefficient, ζ_{bc} is the angle of climb just above the T_{bc} boundary, D_{bc} is the grain size in meters at the T_{bc} boundary, and H_{bc} the ripple height in meters at the T_{bc} boundary. Typical calculated values of R_{bc} range from 0.01 to 0.5 mm/s (Allen, 1971a, 1971b).

Flume experiments by Arnott and Hand (1989) suggest that 0.67 mm/s (4 cm/min), is the minimum suspended-load sedimentation rate (Fig. 15) at which bedload

movement is suppressed for medium-grained (230 μm) sand; this rate is termed R_{ab} , the sedimentation rate at the T_{ab} boundary (Fig. 15). Allen (1991) assumed for simplicity that the sedimentation rate at the T_{cd} boundary, R_{cd} , is effectively zero. Assuming a linear decrease in turbidity current sedimentation rate, Allen (1991) developed equations to estimate the accumulation times, τ_a and τ_b , of the T_a and T_b divisions, respectively:

$$\tau_a = \frac{1}{k} \ln \frac{R_0 + kz_{ab}}{R_0} \quad (4)$$

$$\tau_b = \frac{1}{k} \ln \frac{R_0 + kz_{ab}}{R_0 + kz_{bc}} \quad (5)$$

$$\text{where } k = \frac{R_{ab} - R_{bc}}{z_{ab} - z_{bc}} \quad (6)$$

where z_{ab} and z_{bc} are the heights above the base of the bed of the T_{ab} and T_{bc} boundaries, respectively (Fig. 15). R_0 is the sedimentation rate at the base of the T_a division ($z=0$), R_{ab} and R_{bc} are the sedimentation rates at the T_{ab} and T_{bc} boundaries, respectively (Fig. 15), and k is the linear gradient of R with respect to the bed height.

Baas et al. (2000) modified equations 4 and 5 by incorporating empirical ripple stability data (van den Berg and van Gelder, 1993; Baas, 1994, 1999) into an equation for the length of time to deposit the T_c division. The resultant mathematical model is termed TDURE (Baas et al., 2000; Fig. 15), which has three modules: *Module 1* calculates the accumulation time of the T_a and T_b divisions using equations 4 and 5, respectively (Baas, et al., 2000; Baas, 2004). *Module 2* calculates the accumulation time of the T_c division using ripple measurement data (climb angle ζ , grain size D , ripple height H , and thickness of T_c division z_c) and empirical relationships between ripple migration rate u_r and a grain-

size related mobility parameter θ' derived from the bedform stability diagram of van den Berg and van Gelder (1993) :

$$\tau_c = \frac{X(b+1)(\theta_{cd}' - \theta_{bc}')}{a(\theta_{cd}'^{b+1} - \theta_{bc}'^{b+1})} \quad (7)$$

where τ_c is the duration of the T_c division, X is the total horizontal displacement of a ripple train, and θ'_{bc} and θ'_{cd} are the grain-related mobility parameters at the T_{bc} and T_{cd} boundaries, respectively (Baas et al., 2000). Coefficients a and b are grain-size dependent coefficients that form the scaling factor and exponent, respectively, for the best-fit power function between ripple migration rate u_r and the grain related mobility parameter θ' (Baas et al., 2000):

$$u_r = a\theta'^b \quad (8)$$

The total horizontal displacement of a ripple train X and the ripple migration rate u_r can be found by the following geometrical relationships (Fig. 15):

$$X = \frac{z_c}{\tan\zeta} \quad (9)$$

$$u_r = \frac{R}{\tan\zeta} \quad (10)$$

Module 3 of TDURE compares the expected development of ripple height in the T_c division with the observed change in ripple height. This comparison is based on empirical relationships between the ratio of instantaneous ripple height $H(t)$ to the equilibrium ripple height H_E (Baas, 1994, 1999), the time required to reach equilibrium τ_E , and θ' :

$$\frac{H(t)}{H_E} = 1 - (0.01)^{S_{II}} \quad (11)$$

$$S_H = \left(\frac{\theta'_{bc} - \theta'_{cd}}{c\tau_c} \right)^{\frac{1}{d}} \frac{(\tau_c^{1+\frac{1}{d}} - (\tau_c - t)^{1+\frac{1}{d}})}{1 + \frac{1}{d}} \quad (12)$$

where S_H is the development stage of ripple height, t is the development or accumulation time, and c and d are grain-size dependent coefficients in best-fit power functions for τ_E and θ' , in the form of equation 8. The calculated height at the T_{cd} boundary H_{cd} (Fig. 3) can then be compared to the observed height H to confirm accuracy of the calculations made in Module 2 (Baas et al., 2000). The three modules of TDURE have been incorporated by Baas et al. (2000) into a spreadsheet that largely automates the aforementioned calculations, providing sedimentation rates R_0 , R_{ab} , R_{bc} , accumulation times τ_a , τ_b , τ_c , and the expected ripple height H_{cd} at the T_{cd} boundary for comparative purposes.

6.2. Sedimentation Rates and Accumulation Times Calculated From the Three Locales

Measurements of ripple height H and wavelength λ , angle of climb ζ , grain size D , and thickness of the CRCL deposit z were taken from 44 sedimentation units from the three locales (Table 1). Generally, poor weathering of rock faces in the ZA locale and the inherent limitations of the MAG core restricted the number of measurements that could be made; hence the well-exposed NZ CRCL units provide the bulk of the dataset (Table 1). For all locales, ripple wavelength λ and height H range between 15-25 cm and 5-30 mm, respectively, and average 14.7 cm and 19 mm, respectively (Fig. 16). Ripple indices (λ/H) for the measured CRs range from 3 to 40, averaging 9.5. Climb angle ζ averages 16° , but is broadly distributed between 3° and 50° (Fig. 16). Grain sizes are generally

fine- to very fine-grained ($\sim 105 \mu\text{m}$) sand (Table 1), determined by 45 grain size measurements using a Malvern Mastersizer 2000 particle size analyzer.

H, D, ζ , and z were entered into TDURE (Baas et al., 2000) to calculate the sedimentation rates and accumulation times of each bed (Fig. 17). Without a T_a division, TDURE assigns R_0 as R_{ab} of 0.67 mm/s (Arnott and Hand, 1989; Baas et al., 2000). In the absence of a T_a or T_b division, TDURE uses equation 3 to compute R_0 (assuming deposition begins at the phase boundary between the T_b and T_c divisions) and equation 7 to compute τ_c . Consequently, the calculated values represent maximum sedimentation rate values and minimum accumulation times. Where there is a significant change in ζ within a unit, a separate TDURE calculation was made for each segment. These component calculations were summed to produce a whole-bed averaged sedimentation rate and accumulation time (Fig. 17). CRCL sedimentation rates range from 0.04 to 0.39 mm/s, averaging 0.15 mm/s (Fig. 17A) and CRCL accumulation times range from 3 to 113 minutes, averaging 27 minutes (Fig. 17B). Whole-bed accumulation times, including underlying T_b divisions in Facies 1 beds, range from 3 to 176 minutes and average 35 minutes (Fig. 17C).

Modules 1 and 2 of TDURE calculate sedimentation rates and accumulation times while Module 3 estimates the expected final ripple height H_{cd} to compare with observed ripple height H in order to confirm accuracy of Module 2 calculations. This is based on the assumption that ripple height is independent of sedimentation rate and thus climb angle (review in Baas et al., 2000). However, for the CRCL units measured in this study, there is a positive correlation between ζ and H (Fig. 17D). The most densely sampled NZ-M package clearly shows this relationship, with correlation coefficient $R^2 = 0.62$

(Fig. 17D); trendlines for other locales are not shown in Figure 17D, but show similar trends. These trends may be caused by the large amount of suspended sediment available to the developing CRs, leading to faster equilibration times and thus larger heights. Also, H is generally 5-10 mm higher than H_{cd} (Table 2), suggesting that faster equilibration times allow for a larger ripple to develop during a particular flow event. Thus, independent verification of the Module 2 calculations using Module 3 is not possible in most cases due to the large differences between H and H_{cd} and the positive correlation between ζ and H . Consequently, sedimentation rates shown here are calculated using equation 3 (equation 8 of Baas et al., 2000), which does not depend on the Module 3 calibration.

6.3. Flow Properties Compared Among Facies

Since Facies 1 includes T_b divisions, whole-bed sedimentation rates are reported, averaging 0.24 ± 0.07 mm/s (Table 2). CRCL sedimentation rates in Facies 2 averaged 0.14 ± 0.07 mm/s overall, 0.10 mm/s in the NZ locale, 0.24 mm/s in the ZA locale, and 0.14 mm/s in the MAG locale (Fig. 17A, Table 2). The large values in Facies 1 are expected, as TDURE assumes a linear decrease in sedimentation rate through successive turbidite divisions (Baas et al., 2000). The ZA locale shows the highest Facies 2 CRCL sedimentation rate, interpreted to result from slightly larger grain size and steep climb angle values. Accumulation times in Facies 2 average 27 minutes and range from 15-60 minutes, depending on bed thickness (Fig. 17). Facies 1 beds are generally thicker and hence show longer accumulation times, averaging 46 minutes and values up to 176 minutes for very thick beds (Fig. 17B). To normalize these accumulation times for

comparison, beds of ~ 50 cm thickness of both Facies 1 and 2 were isolated; this subset of Facies 1 beds averaged 40 minutes while Facies 2 beds averaged 26 minutes.

6.4. Stratigraphic Changes in Sedimentation Rate

Accumulation times vary widely due to variations in bed thickness and facies distribution, but are not consistently higher in one locale than another (Figs. 17B, C). CRCL sedimentation rates do not vary widely between the NZ, ZA, and MAG locales, averaging close to 0.15 mm/s (Fig. 17A). However, within the NZ locale, where sample sizes are large enough for valid comparison, distinct stratigraphic trends in CRCL sedimentation rates are apparent. In the NZ-M sub-locale, CRCL sedimentation rates are initially low but progressively increase upward stratigraphically (Fig. 17A). Beds NZ-M-1 to NZ-M-6 were deposited in an overbank setting (Figs. 11A, 14A) and have low CRCL sedimentation rates, averaging 0.07 mm/s (Fig. 17A). Beds NZ-M-8 to NZ-M-17 lie above the channel truncation surface (Fig. 11B) and show higher CRCL sedimentation rates, averaging 0.14 mm/s (Fig. 17A). The NZ-M and NZ-S sub-locales are separated by a covered interval and a small-offset fault, but NZ-S CRCL sedimentation rates are very similar (average 0.17 mm/s) to the upper NZ-M rates, suggesting that the M to S transition is arbitrary and due predominantly to exposure constraints. The progressive increase in sedimentation rate (Fig. 17A) in the upper NZ-M and NZ-S beds is interpreted to result from an increase in turbidity current frequency and magnitude associated with channel development.

6.5. Comparisons With Other Studies

This study calculated average CRCL sedimentation rates of 0.15 mm/s and average accumulation times of 27 minutes. CRCL sedimentation rates measured by Allen (1971a) from both flume and outcrop studies range from 0.001 to 0.1 mm/s and accumulation times of 11 minutes to 35 hours. Given that bed thicknesses, grain sizes, and climb angles vary considerably between studies (Fig. 16), these estimates are similar. Ashley et al. (1982) performed flume experiments of CRs using 150 μm natural quartz sand and measured average sedimentation rates of 0.025 mm/s, about an order of magnitude lower than those calculated in this study. While arbitrarily derived, the 30-200 minute flow duration values of Ashley et al. (1982) produce very similar CRCL thicknesses and geometries to those in this study. Flume runs 1 and 2 (Arnott and Hand, 1989) contained supercritical climbing ripples with $\zeta \sim 35^\circ$ with sedimentation rates of 0.25 to 0.43 mm/s, which agree well with supercritical climbing ripples in our study (e.g. NZ-N-10, ZA-6-25). The natural 'Doheny' turbidite studied by Allen (1991) had a sedimentation rate (R_{bc}) of 0.275 mm/s and a range of 20-52 minutes for the accumulation time. For the same turbidite, Baas et al. (2000) calculated a CRCL-only sedimentation rate (R_{bc}) of 0.27 mm/s and a CRCL accumulation time of 12 minutes. Baas (2004) used TDURE to perform 167 turbidite simulations, the accumulation time of the T_c division ranging from 0.3 to 39 minutes and CRCL sedimentation rates ranging from 0.001 to 0.3 mm/s. Flow durations for natural turbidity currents range from several hours for the 1929 Grand Banks current (Heezen and Ewing, 1952) up to several days for currents traversing the Amazon submarine channel (Pirmez and Imran, 2003). It is important to note, however, that the accumulation time of a turbidite may not accurately reflect the total duration of the depositing flow.

7. THE INFLUENCE OF GRAIN SIZE ON THE FORMATION OF CLIMBING RIPPLES

Climbing ripples in general and those in each of the three studied locales consist predominantly of very fine- to fine-grained sand (Table 1). It is clear from the geological record and flume studies (Allen, 1971a; Stanley, 1974; Southard and Boguchwal, 1990) that CRCL-rich deposits similar to those in this study are rare to nonexistent in systems dominated by medium- and coarse-grained sand. However, empirical data (Southard and Boguchwal, 1990) show that non-climbing current ripples are stable in grain sizes up to approx. 750 μm (coarse-grained sand). Therefore, something must discourage the formation of CRCL in coarser grain sizes. The following section discusses the influence of grain size on suspended load fallout rates at various concentrations and the potential impacts on CRCL formation.

Dense settling sediment suspensions display hindered settling whereby the fall velocity of uniformly sized particles in a suspension, U_{susp} , is reduced from the fall velocity of a single particle at infinite dilution, U_0 . Maude and Whitmore (1958) expressed this relationship by:

$$U_{\text{susp}} = U_0 (1-C)^n \quad (13),$$

where C is equal to the volume concentration of particles and n is an empirically derived exponent that is a function of the grain Reynolds number and varies from 4.65 for particles settling viscously to 2.4 for inertial particles (Maude and Whitmore, 1958). Fine- and very fine-grained sand settles largely under viscous conditions while medium sand is transitional ($n = 3.525$) and coarse grained sand settles inertially ($n = 2.4$)

(Richardson and Zaki, 1954; Maude and Whitmore, 1958). The difference between U_{susp} and U_0 is relatively greater for finer grained sand because of the larger value of n , indicating that hindered settling affects very fine and fine sand more than coarser grains (Fig. 18), allowing more sediment to be carried in suspension as compared to coarser grain sizes.

During deposition of a suspension of uniformly sized particles, the settling velocity of the suspension and the rate of bed rise is given by:

$$(U_{\text{susp}}) (C_{\text{susp}}) = (U_{\text{bed}}) (C_{\text{bed}}) \quad (14)$$

where U_{susp} is the settling velocity of the suspension, C_{susp} is the concentration of the settling suspension, U_{bed} is the rate of bed rise, which is equivalent to the sedimentation rate R discussed above, and C_{bed} is the volumetric concentration of particles in the bed, which we will assume is 70%, similar to many uncompacted sands (Hedberg, 1926). Using hindered settling velocities calculated using equation 13, Figure 18 displays the U_{bed} sedimentation rates for different values of C_{susp} for very fine-, fine-, medium-, and coarse-grained sand. For very fine-grained sand, the sedimentation rates at $C=1\%$ and $C=2.5\%$ (Fig. 18) are quite similar to those calculated by TDURE, which average 0.15 mm/s (Fig. 17A; Table 2). For fine-grained sand at $C=1\%$, U_{bed} is 0.23 mm/s, also similar to the Facies 2 rates in ZA of 0.24 mm/s (Fig. 17A). At C_{susp} values higher than 2.5%, U_{bed} for fine-grained sand is greater than the bedload suppression rate of $R_{\text{ab}} = 0.67$ mm/s (Fig. 18), suggesting that settling sediment may accumulate without bedload movement, forming a T_a division. For very fine sand, however, R_{ab} is not reached until $C_{\text{susp}} \geq 20\%$ (Fig. 18), indicating a wide concentration range over which CRCL will form. These U_{bed} values suggest that for very fine- and fine-grained sand at concentrations less

than 20% and 2.5% respectively, hindered settling provides a sedimentation rate approximately equal to that needed to deposit CRCL (Fig. 18). These predicted particle concentrations for CRCL deposition are similar to published estimates of particle concentrations in low-density turbidity currents (e.g., Lowe, 1982; Prior et al., 1987; Johnson et al., 2001b). On the other hand, U_{bed} values for medium and coarse sand, even at $C_{susp} = 1\%$, are greater than the bedload suppression rate R_{ab} (0.67 mm/s) observed by Arnott and Hand (1989), leading to the formation of a T_a or $S3$, using terminology of Lowe (1982), division. These observations may help to explain the common appearance of CRCL in fine-grained turbidite systems and the predominance of $T_a/S3$ divisions and relative lack of CRCL deposits in coarse-grained turbidite systems.

8. APPLICATION TO HYDROCARBON EXPLORATION

Empirical data show that massive, unorganized sands, such as the T_a division of turbidites, generally perform as the best reservoirs while bed load transport, such as in T_b or T_c divisions, forms laminations of varying grain size and better sorts and packs grains, causing decreased porosity and permeability (Dreyer et al., 1990; Spain, 1992; Doyle and Sweet, 1995). Thin-bedded CRCL deposits are therefore not considered to be optimal reservoirs for hydrocarbons due to micro-scale heterogeneity caused by the fine grain size ($< 200 \mu\text{m}$), poor sorting, and the deposition of low-permeability platy mica and clay particles on lamination, ripple trough, and climb surfaces. Furthermore, CRCL are commonly deposited in off-axis depositional environments where significant amounts of mud also accumulate between events. These factors, combined with fault-related heterogeneity, has led to the intense compartmentalization of the Magnolia field, as

observed in studies based on reservoir pressure and fluid phase (Weissenburger and Borbas, 2004; McCarthy et al., 2005, 2006).

Consequently, it can be expected that CRCL-rich reservoirs will exhibit decreased vertical and horizontal permeability and poor well communication compared to reservoirs composed of massive, coarser grained facies. In the NZ locale, the non-amalgamated facies and mudstone-lined channel truncation surfaces (Fig. 11) act to exacerbate reservoir heterogeneity. However, this heterogeneity can be minimized by the presence of scours such as those observed in the ZA and MAG locales that cause amalgamation (Fig. 12; Morris et al., 2000). Lastly, the presence of CRCL-rich facies can be used predictively in depositional environment interpretation. If the local topographic configuration and average flow direction is known or can be inferred, the presence of CRCL in off-axis settings can be used to predict the proximity of scoured and axial environments where higher quality reservoirs may be encountered (see Figs. 9, 14).

8. CONCLUSIONS

This study is the first to focus on the depositional environments and flow properties for climbing-ripple cross-laminated (CRCL) units deposited by turbidity currents. Three locales with thick (> 50 m) CRCL-dominated intervals were studied in detail to clarify depositional architecture and flow properties: The Miocene Upper Mount Messenger Formation, Taranaki Basin, New Zealand; The Permian Skoorsteenbergh Formation in the Tanqua depocenter of the Karoo basin, South Africa; and lower Pleistocene deposits of the Magnolia Field in the Titan basin, Gulf of Mexico. Four CRCL facies were identified from these areas based on bed thickness and CRCL

morphology and changes in the angle of climb. These facies represent an upslope to downslope evolution of CRCL flows within a depositional environment conducive to CRCL development. Proportions of these facies and other contextual observations indicate that the CRCL in the New Zealand locale were deposited both out-of-channel and intra-channel in off-axis, marginal positions while CRCL in the South Africa locale and the Magnolia field were deposited relatively far from confinement in off-axis depositional settings. The recurring feature in each of these off-axis depositional settings is the presence of topography that causes flow non-uniformity, such as a decrease in gradient and/or loss of confinement.

To support these interpretations, 44 beds from the three locales were analyzed using TDURE, a mathematical model of turbidity current sedimentation rate and accumulation time developed by Baas et al. (2000). TDURE calculations validate our facies designations and indicate that average CRCL sedimentation rates across the three locales were 0.15 mm/s and average accumulation times were 27 minutes. Too few measurements were made to compare rates within the South Africa and Magnolia locales. In the New Zealand locale, however, a clear trend of increasing sedimentation rates is seen in stratigraphic proximity to channel-fill intervals. Higher sedimentation rates occur in intra-channel positions due to larger, longer or more frequent flows. Similar patterns of CRCL sedimentation may be expected in other channel-fill successions.

The formation of CRCL is strongly grain size dependent, and all three locales consist predominantly of very fine- to fine-grained sand. The TDURE-calculated sedimentation rates of 0.15 mm/s correlate well with the rate of sedimentation due to hindered settling of suspensions of very fine- and fine-grained sand at concentrations up

to 20% and 2.5%, respectively. These predicted particle concentrations for CRCL deposition are similar to published concentration estimates for low-density turbidity currents (e.g., Lowe, 1982; Prior et al., 1987; Johnson et al., 2001b). For medium- and coarse-grained sand, hindered settling rates at all concentrations are high enough to suppress bedform development and likely result in the formation of massive T_a or S_3 divisions.

The formation of CRCL in turbidite depositional environments therefore requires a narrow grain size range and commonly occurs in areas of flow non-uniformity. A hydraulic jump, an abrupt decrease in gradient, and/or a decrease in confinement, either at a channel mouth or by flow stripping are all common ways to cause flow non-uniformity. These changes in the flow boundary conditions promote flow velocity and thickness reductions and flow expansion/divergence, leading to suspended-load fallout and thus extensive CRCL deposition.

9. ACKNOWLEDGEMENTS

Funding for this field research comes primarily from the Stanford Project On Deepwater Depositional Systems (SPODDS) industrial affiliates program, which includes Aera, Anadarko, Chevron, ConocoPhillips, Devon, ENI-AGIP, ExxonMobil, Hess, Marathon, Nexen, Occidental, Petrobras, Reliance, Rohöl-Aufsuchungs AG (R.A.G.), and Shell. The Department of Geological and Environmental Sciences at Stanford University also provides additional financial support through fellowships and teaching assistantships. Special thanks go to ConocoPhillips and Juli Ericsson for financing ZA field work and permission to release MAG data. Deville Wickens and family were

instrumental in the success of South African field work, and Poppie Cloete was a motivated and perceptive field assistant. GNS New Zealand and Peter King are acknowledged for their support in NZ; Anne Bernhardt and Melanie Stiegler were fantastic field assistants. Jaco Baas kindly gave me the TDURE model and offered invaluable advice on data quality. Many discussions with Zoltan Sylvester have led to the formation of key ideas; he also analyzed grain size data. This study has profited from insightful discussions with DeVille Wickens, Peter King, Geoff Haddad, Mark Ahlert, Dave McGee, Amy Kwiatkowski, Steve Graham, Gary Parker, Anne Bernhardt, Dominic Armitage, Jake Covault, Brian Romans, Katie Maier, Chris Mitchell, and many other SPODDS geologists. Finally, we are especially appreciative of the guidance and lucidity provided by the reviewers of the manuscript: Dave Rubin, Jaco Baas, and Stephen Rice.

10. DEFINITION OF SYMBOLS

ζ	angle of climb
ζ_{bc}	angle of climb at the T_{bc} boundary
ζ_{cd}	angle of climb at the T_{cd} boundary
θ'	grain-related mobility parameter
θ'_{bc}	grain-related mobility parameter at the T_{bc} boundary
θ'_{cd}	grain-related mobility parameter at the T_{cd} boundary
λ	ripple wavelength
μ	dynamic fluid viscosity
ρ_f	fluid density
τ_a	accumulation time for the T_a division
τ_b	accumulation time for the T_b division
τ_c	accumulation time for the T_c division
τ_E	time to reach H_E , the equilibrium ripple height

a	grain-size dependent scaling factor for the u_r and θ' power law function
b	grain-size dependent exponent for the u_r and θ' power law function
c	grain-size dependent scaling factor for the τ_E and θ' power law function
C	volumetric concentration
C_{bed}	volumetric concentration of the bed layer
C_{susp}	volumetric concentration of the suspended-load

CR	abbreviation for climbing ripple(s)
CRCL	abbreviation for climbing-ripple cross-lamination
d	grain-size dependent exponent for the τ_E and θ' power law function
D	grain size
D_{bc}	grain size at the T_{bc} boundary
H	ripple height (observed)
H_{bc}	ripple height at the T_{bc} boundary
H_{cd}	ripple height at the T_{cd} boundary
H_E	equilibrium ripple height
$H(t)$	ripple height at time t
j_b	bedload transport rate
k	linear gradient of R with respect to the bed height
L	length term for Reynolds number, here defined as flow depth
n	grain-size dependent, empirically derived exponent varying between 2.4 and 4.65
NZ	abbreviation for New Zealand
MAG	abbreviation for Magnolia Field
Q_B	sediment flux from reattachment point erosion
Q_S	sediment flux from suspended load
R	suspended load fallout rate
R_0	initial suspended load fallout rate
R_{ab}	suspended load fallout rate at the T_{ab} boundary
R_{bc}	suspended load fallout rate at the T_{bc} boundary
R_{cd}	suspended load fallout rate at the T_{cd} boundary
Re	Reynolds number
S_H	development stage of ripples
t	time
u_r	ripple migration rate
U_0	fall velocity of a single particle at infinite dilution
U_{bed}	rate of bed rise
U_{susp}	fall velocity of particles from the suspended load (cf. R)
v	flow velocity
X	horizontal displacement of a ripple train
z_{ab}	height above the bed base of the T_{ab} boundary
z_{bc}	height above the bed base of the T_{bc} boundary
z_{cd}	height above the bed base of the T_{cd} boundary
z_c	thickness of the T_c division
ZA	abbreviation for South Africa


Table 1. CRCL measurements from 44 sedimentation units from the three locales.

Locale	Bed	Grain size D (μm)	Ripple Height H (mm)	Ripple Wave-length λ (cm)	Climb angle ζ ($^{\circ}$)	T_b thickness (cm)	T_c thickness (cm)	Total bed thickness (cm)
NZ-wai	1	105	20	12	5	-	5	5
NZ-wai	2	105	20	19	8	-	8	8
NZ-N	1	105	18	14.5	18	5	16	21
NZ-N	2a	105	13	7	12	10	10	20
NZ-N	2b	105	25	16.5	8	-	8	8
NZ-N	3a	105	9	7	7	50	2	52
NZ-N	3b	105	35	19.5	11	-	18	18
NZ-N	4	105	20	10.5	22	5	15	20
NZ-N	5	105	5	20	7	8	13	21
NZ-N	6	105	21	13	14.5	10	12	22
NZ-N	7	105	10	13	9	5	11	16
NZ-N	8	105	10	14	11.5	5.5	9	14.5
NZ-N	9	105	25	15	20	14	27	41
NZ-N	10	105	8	8	14	-	5	5
NZ-N	11	105	25	12.5	14	20	35	55
NZ-N	12	105	31	11.5	15.5	-	20	20
NZ-M	1	105	15	22	3.5	85	37	122
NZ-M	2	105	17	16	5	-	10	10
NZ-M	3a	105	15	11.5	6	-	5	5
NZ-M	3b	105	15	11.5	6	10	8	18
NZ-M	4	105	15	14	4.3	-	5	5
NZ-M	5a	105	12	10.5	8	145	32	177
NZ-M	5b	105	25	15.5	22	-	10	10
NZ-M	6	105	26	12.6	11.8	10	12	22
NZ-M	8	105	15	10.8	10.5	-	32	32
NZ-M	9a	105	10	11.5	7	53	9	62
NZ-M	9b	105	8	9.3	10	11	4	15
NZ-M	10a	105	12	14	12	45	3	48
NZ-M	10b	105	9	9	5	4	4	8
NZ-M	10c	105	13	8.5	12	1	6	7
NZ-M	10d	105	40	26	20	-	6	6
NZ-M	10e	105	50	29	30	-	2	2
NZ-M	11	105	34	16	19	-	14	14
NZ-M	12	105	21	13	12	-	12	12
NZ-M	13	105	15	15	8.5	60	60	120
NZ-M	14	105	24	17	28	-	10	10
NZ-M	15a	105	5	10	8	-	8	8
NZ-M	15b	105	12	12	15	70	50	120
NZ-M	16	105	22	15	19	-	42	42
NZ-M	17	105	25	18	16	-	37	37
NZ-S	1	105	25	13.5	28	-	85	85
NZ-S	2a	105	13	9	4	10	12	22
NZ-S	2b	105	16	11	8	-	15	15
NZ-S	2c	105	19	15.5	21	-	15	15
NZ-S	2d	105	22	12.5	48	-	19	19
NZ-S	2e	105	20	12	25	-	21	21
NZ-S	3	105	25	27	16	-	48	48
NZ-S	4	105	23	15	13	-	35	35
NZ-S	5	105	22	11	28	-	110	110
ZA-1	12m	149	25	19.5	24	-	200	200
ZA-6	25m	105	12	22	25	-	20	20
ZA-6	37m C	105	10	16	6.2	-	50	50
ZA-6	37m D	105	10	16	30.4	-	50	50
ZA-7	13m	105	16	9	22	-	50	50
ZA-14	12m	105	13	19	15	-	90	90
Mag	18809	84	20	15	22	-	9.1	9.1
Mag	18811	84	18	15	12	-	6.1	6.1
Mag	18815	84	10	15	17	-	30.5	30.5
Mag	18781	84	15	15	12.8	-	45.7	45.7

Table 2. TDURE calculations from 44 sedimentation units from the three locales.

Locale	Bed	CRCL sedimentation rate (mm/s)	CRCL accumulation time (min)	Whole bed averaged sedimentation rate (mm/s)	Whole bed accumulation time (min)	S _H development stage	Predicted H _{cd} (mm)
NZ-wai	1	0.04	10.74	0.08	10.74	0.67	12.91
NZ-wai	2	0.07	10.7	0.12	10.70	0.67	12.90
NZ-N	1	0.18	9.26	0.38	9.26	0.58	12.58
NZ-N	2	0.11	19.54	0.19	24.17	0.67	12.90
NZ-N	3	0.10	20.47	0.26	45.23	0.88	12.90
NZ-N	4	0.20	6.98	0.44	9.10	0.44	11.71
NZ-N	5	0.25	19.9	0.15	23.04	1.24	13.48
NZ-N	6	0.12	8.72	0.31	11.75	0.54	12.42
NZ-N	7	0.16	13.05	0.17	15.39	0.81	13.21
NZ-N	8	0.21	8.31	0.28	10.65	0.52	12.29
NZ-N	9	0.15	13.94	0.39	20.71	0.87	13.28
NZ-N	10	0.31	3.77	0.22	3.77	0.24	8.95
NZ-N	11	0.10	26.39	0.24	37.48	1.65	13.52
NZ-N	12	0.09	13.56	0.25	13.56	0.85	13.25
NZ-M	1	0.04	113.71	0.12	176.55	7.10	13.53
NZ-M	2	0.05	21.48	0.08	21.48	1.34	13.50
NZ-M	3	0.07	23.25	0.13	29.50	0.56	12.49
NZ-M	4	0.05	12.5	0.07	12.50	0.78	13.15
NZ-M	5	0.14	47.45	0.25	123.41	2.67	13.53
NZ-M	6	0.08	10.8	0.22	16.77	0.67	12.92
NZ-M	8	0.12	32.45	0.16	32.45	2.03	13.52
NZ-M	9	0.17	18.04	0.26	49.85	0.86	13.27
NZ-M	10	0.13	20.3	0.29	43.17	0.25	8.09
NZ-M	11	0.10	7.64	0.31	7.64	0.48	12.02
NZ-M	12	0.10	10.61	0.19	10.61	0.66	12.89
NZ-M	13	0.10	75.46	0.18	108.76	4.71	13.53
NZ-M	14	0.22	3.54	0.47	3.54	0.22	8.63
NZ-M	15	0.25	45.77	0.29	74.36	2.19	13.52
NZ-M	16	0.16	22.93	0.31	22.93	1.43	13.51
NZ-M	17	0.12	24.25	0.25	24.25	1.51	13.51
NZ-S	1	0.21	30.05	0.47	30.05	1.88	13.52
NZ-S	2	0.22	71.34	0.20	78.14	0.89	11.88
NZ-S	3	0.12	31.46	0.25	31.46	1.96	13.52
NZ-S	4	0.10	28.5	0.20	28.50	1.78	13.52
NZ-S	5	0.24	38.89	0.47	38.89	2.43	13.52
ZA-1	12m	0.18	84.43	0.39	84.43	5.27	13.53
ZA-6	25m	0.39	8.06	0.41	8.06	0.50	12.19
ZA-6	37m	0.35	102.53	0.16	102.53	5.40	13.53
ZA-7	13m	0.26	23.26	0.36	23.26	1.45	13.51
ZA-14	12m	0.21	63.13	0.24	63.13	3.94	13.53
Mag	18809	0.15	3.37	0.45	3.37	0.24	8.36
Mag	18811	0.09	4.3	0.24	4.30	0.30	9.45
Mag	18815	0.22	14.93	0.34	14.93	1.05	12.48
Mag	18781	0.11	30.11	0.25	30.11	0.70	12.08

Figure 1. Ripple morphology and terminology (modified from Jopling and Walker, 1968, Allen, 1971a). Under normal bedload transport conditions, the lee and stoss sides of current ripples are depositional and erosional, respectively. Climbing occurs when suspension sedimentation reduces or suppresses reattachment point erosivity.

Flow 

← Wavelength →

← Lee side →

← Stoss side →

← Lee side →

Flow expansion

Flow contraction

1-3 cm

Reattachment point

Crest

Flow streamlines

Separation bubble

Height

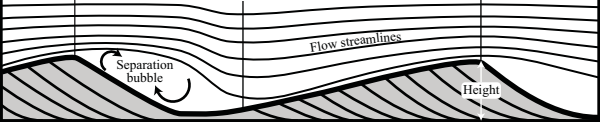


Figure 2. Climbing-ripple cross-lamination (CRCL) nomenclature and classification. CRCL deposits can be classified according to the critical angle of climb, where stoss-side erosion occurs. CRCL with low climb angles and stoss-side erosion are ‘subcritical’ while CRCL with higher climb angles and stoss-side preservation are ‘supercritical.’ Sinusoidal, or wavy, lamination occurs at very high climb angles and high suspension fallout rates and is essentially an aggrading bedform. The increasing angle of climb indicates an increasing rate of suspension sedimentation and/or decreasing rate of bedform migration. Figure modified from Hunter (1977); climb angle ranges and thicknesses are approximate.

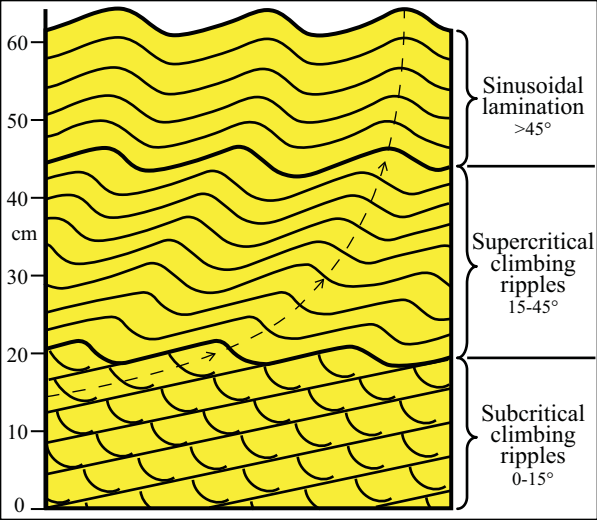


Figure 3. Locations of the three study areas. A general location map of each is shown: New Zealand (NZ) is shown in **(A)**, Magnolia (MAG) in **(B)**, and South Africa (ZA) in **(C)**; boxes denote locations of more detailed figures.

(D) Tanqua depocenter, Karoo basin, South Africa – for location, see **(B)**.

Skoorsteenberg Formation outcrops shown in grey. ‘Fan 3’ average paleocurrents are shown with red arrows and the approximate boundary of the fan with a dashed line. The solid box shows the location of Figure 12 and the Fan 3 CRCL deposits at the Kleine Reit Fontein locale. Modified from Johnson et al. (2001), Hodgson et al. (2006), and Prelat et al. (2009).

(E) The Titan mini-basin in the Gulf of Mexico, showing the location of Magnolia field. Black box denotes the location of Figure 13 and red arrows are generalized sediment dispersal patterns. Note the location of Magnolia near the southern exit of the Titan basin.

(F) The Mount Messenger (red) and Urenui (green) formations outcrop along the Taranaki coast, North Island, New Zealand; gentle southwesterly dips reveal stratigraphy younging to the south. The Upper Mt. Messenger Formation at Pukearuhue Beach (inset) is the CR locale in this study. NZ-M is the measured section while NZ-N and NZ-S are the older and younger CRCL sublocales where individual bed measurements were made. See Figure 11 for outcrop description.

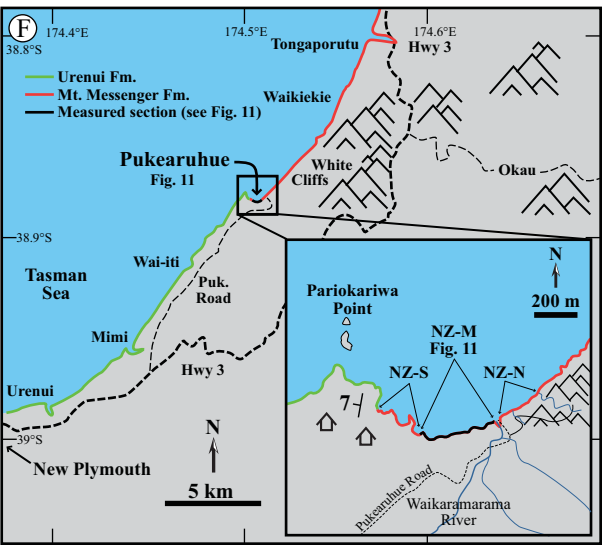
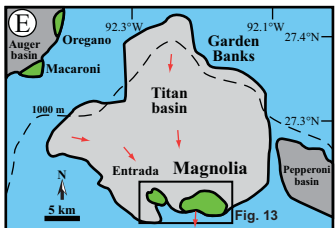
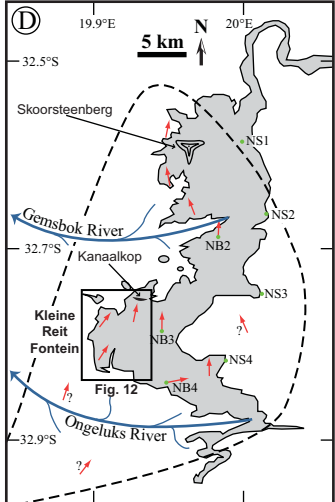
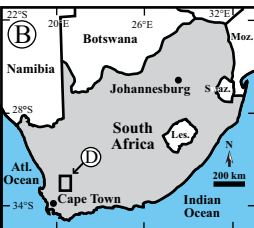


Figure 4. Climbing ripple facies defined by this study. All facies depicted at the same scale.

(A) *Facies 1: Long-lived, surging flows.* These units were deposited by flows with one to several surges that deposited T_b divisions before waning and depositing CRCL with increasing climb angle. Note that the thickness of the basal T_b division can be up to 1.2 m.

(B) *Facies 2: Collapsing flows.* Consists of one sedimentation unit of increasing-climb-angle CRCL that records the increasing suspension fallout rate of a waning, collapsing flow.

(C) *Facies 3: intermediate, waning flows.* Similar to Facies 2, but the vertical evolution of CRCL is incomplete and average bed thickness is much smaller.

(D) *Facies 4: Distal, slow-moving, small-volume flows.* The low climb angles, thin-bedded nature, and interbedded mudstones of Facies 4 indicates that the depositing flows had low sedimentation rates and accumulation times; Facies 4 was likely deposited in relatively distal environments.

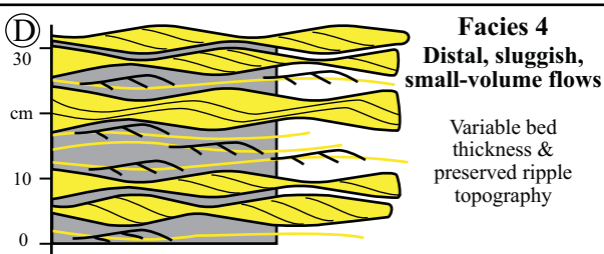
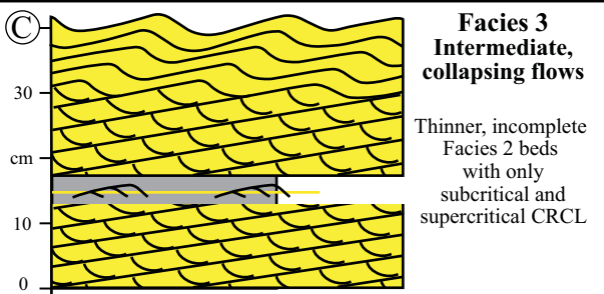
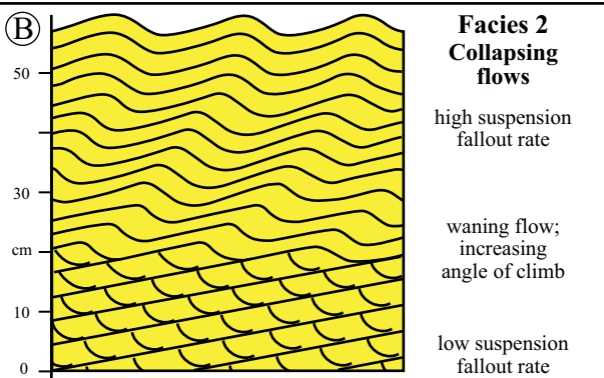
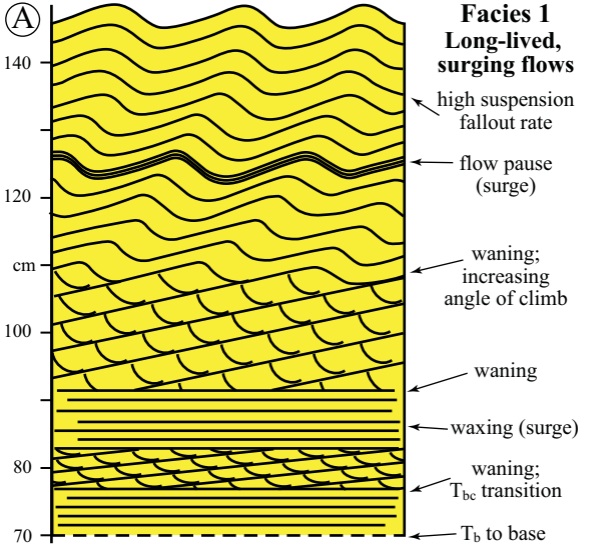


Figure 5. Field example of Facies 1, long-lived surging flows, from Pukearuhue Beach, NZ. The depositing flow had at least 3 surges (noted at right). High-velocity plane lamination extends below the photo for approximately 50 cm. Subcritical CRCL developed in the lower surges, and the final surge contains CRCL of increasing climb angle, representing the final waning of the flow. This unit is NZ-M-10 (Table 1).



T_{cr}

T_e

T_d

T_{cr}

T_b

T_{cr}

T_b

T_{cr}

T_b

NZ
15 cm

Figure 6. Field examples of Facies 2, collapsing flows. (A) and (B) are approximately the same scale; in all photos, flow was from left to right.

(A) Facies 2 from the NZ locale. A small Tb division occurs initially, followed by CRCL of increasing climb angle, representing a flow that due to collapse had ever-increasing suspension fallout rates. This unit is NZ-S-2 (Table 1). Divisions on Jacob staff are 10 cm.

(B) Facies 2 sedimentation unit from the ZA locale. Note the drastic increase in climb angle about halfway up through the bed, representing an abrupt collapse of the flow. This unit is ZA-6-37 (Table 1).

(C) Facies 2 from 18,779 feet (5,723.8 m) in the Magnolia (MAG) core; normal light on the left, ultraviolet light on the right (yellow color is due to presence of hydrocarbons in sand). Note the increase in climb angle through this bed and the vertical aggradation of sinusoidal lamination at the top of the bed. This unit is MAG-18781 (Table 1).

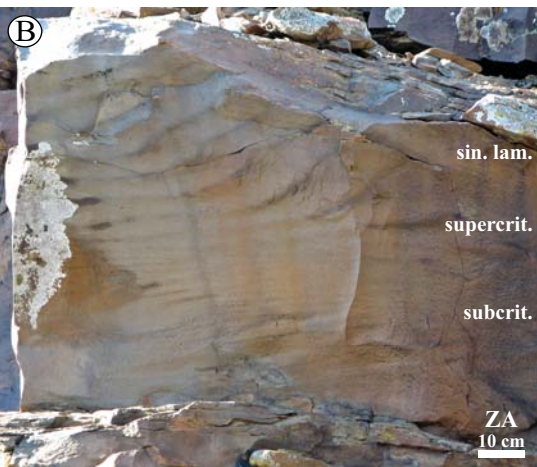
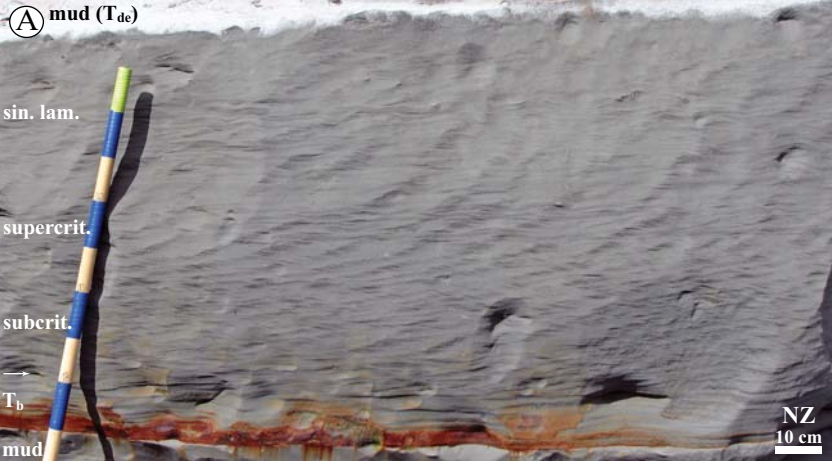


Figure 7. Field examples of Facies 3, intermediate waning flows.

(A) Facies 3 in the NZ locale (NZ-M-11, Table 1). A basal subcritical CRCL division is overlain by supercritical CRCL, indicating an increasing angle of climb, but beds are thinner than in Facies 2 and there is not a well-developed sinusoidal lamination division.

(B) Facies 3 from the ZA locale; note the similar bed thickness to (A). Increasing angle of climb CRCL in this bed indicates a waning flow.

(C) Facies 3 from 18,820 feet (5,736.3 m) in the Magnolia (MAG) core; normal light on the left, ultraviolet light on the right (yellow color is due to presence of hydrocarbons in sand). Note the thin-bedded, mostly subcritical CRCL present, indicating waning flows with relatively low rates of suspension fallout.

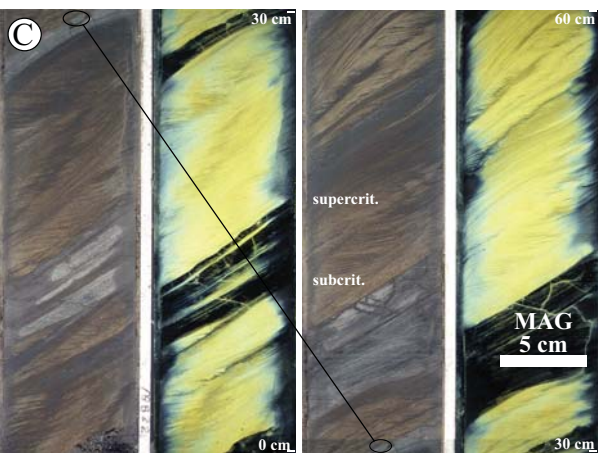


Figure 8 Field example of Facies 4, distal, slow-moving, small-volume flows.

(A) Facies 4 CR deposits at Pukearuhue Beach, New Zealand (NZ). Sand is light-colored, iron-stained, and contains CRs. Mud draping the ripple topography is dark grey and lightly bioturbated.

(B) Facies 4 well developed in the Tanqua Karoo, South Africa (ZA). Note the wavy bed contacts and draped mudstone units. Note that only one flow in this succession (white arrow at right) was robust enough to erode a flat surface before depositing CRCL; it is also thicker than the surrounding beds.

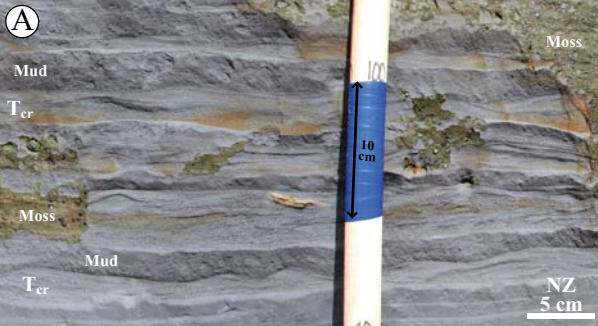


Figure 9. Idealized temporal and downslope facies evolution. Facies 1 is deposited proximally, soon after a flow experiences some sort of non-uniformity such as a gradient change, unconfinement, flow expansion, or flow thickness reduction via flow stripping. As flows progressively decelerate, Facies 2 and 3 are deposited, yielding a flow with little suspended sand load. Facies 4 is therefore deposited in the most distal regions where flows decline and end. Scour depth and frequency also decrease distally and laterally from the axis of flow.

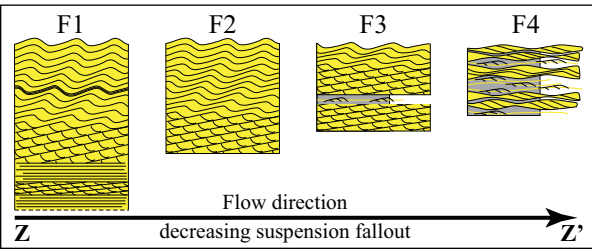
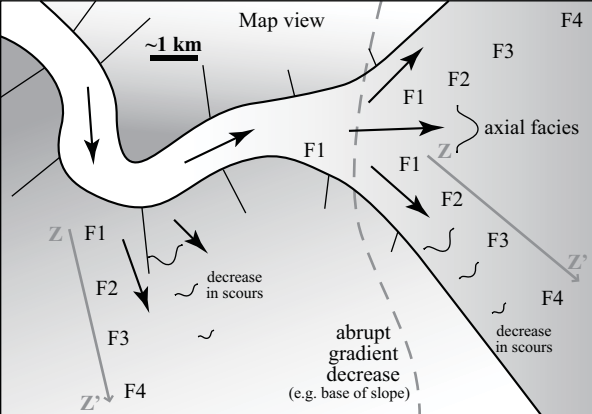
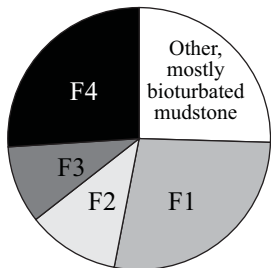


Figure 10. Facies proportions in the three locales. At left are original facies proportions, including non CRCL facies (e.g., channel fill, mudstone) and at right are normalized facies proportions. NZ is rich in Facies 1, indicating that flows had high Reynolds numbers and thus were fully or quasi-confined. ZA and MAG, on the other hand, are rich in Facies 2 and 3, indicating that flows were collapsing, likely due to their totally unconfined nature.

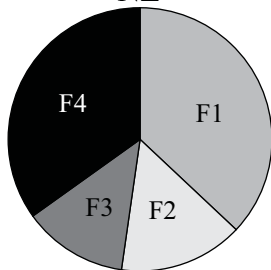
Original

Normalized

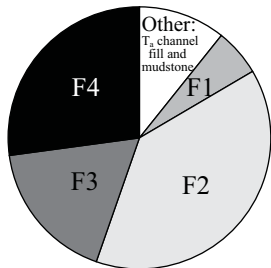
NZ



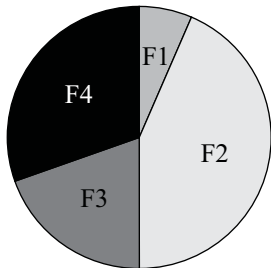
NZ



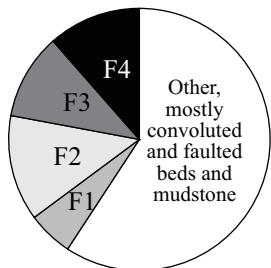
ZA



ZA



MAG



MAG

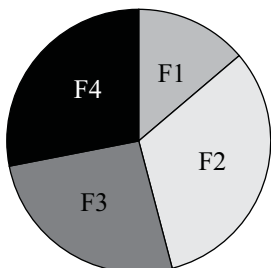


Figure 11. Characterization of the NZ locale.

(A) Measured section of the CRCL deposits at Pukearuhue Beach. Red lines are truncation surfaces; note the abundant bioturbated mudstone above the surfaces. Paleocurrents shown for individual beds in black arrows and corresponding numbers are NZ-M beds in Table 1.

(B) Photopanel documenting the NZ-M measured section; red lines are equivalent to those in (A). Note geologists and Jacob staff for scale near 43 m.

(C) Photo of NZ-M bed #11, demonstrating the increase in climb angle and the interbedded, bioturbated mudstone. Note the sinusoidal lamination at top, indicative of a high suspension fallout rate. Pencil for scale.

(D) Plan view of the simple, straight crested CRs of the NZ locale. Note the easterly paleocurrent direction of this bed, NZ-M bed #18. Divisions on Jacob staff are 10 cm.

(E) Characterization of the truncation surface at 53 m; see (A) for location. Note the erosional and irregular nature of the surface and the intensely bioturbated mudstone above the surface. Divisions on Jacob staff are 10 cm.

(F) Bioturbated mudstone infilling the 6 m truncation surface; see (B) for location. Intense bioturbation has homogenized this interval, and nearly all sand beds are disarticulated. Laminated, relatively undisturbed sandstone is at center. Pencil for scale.

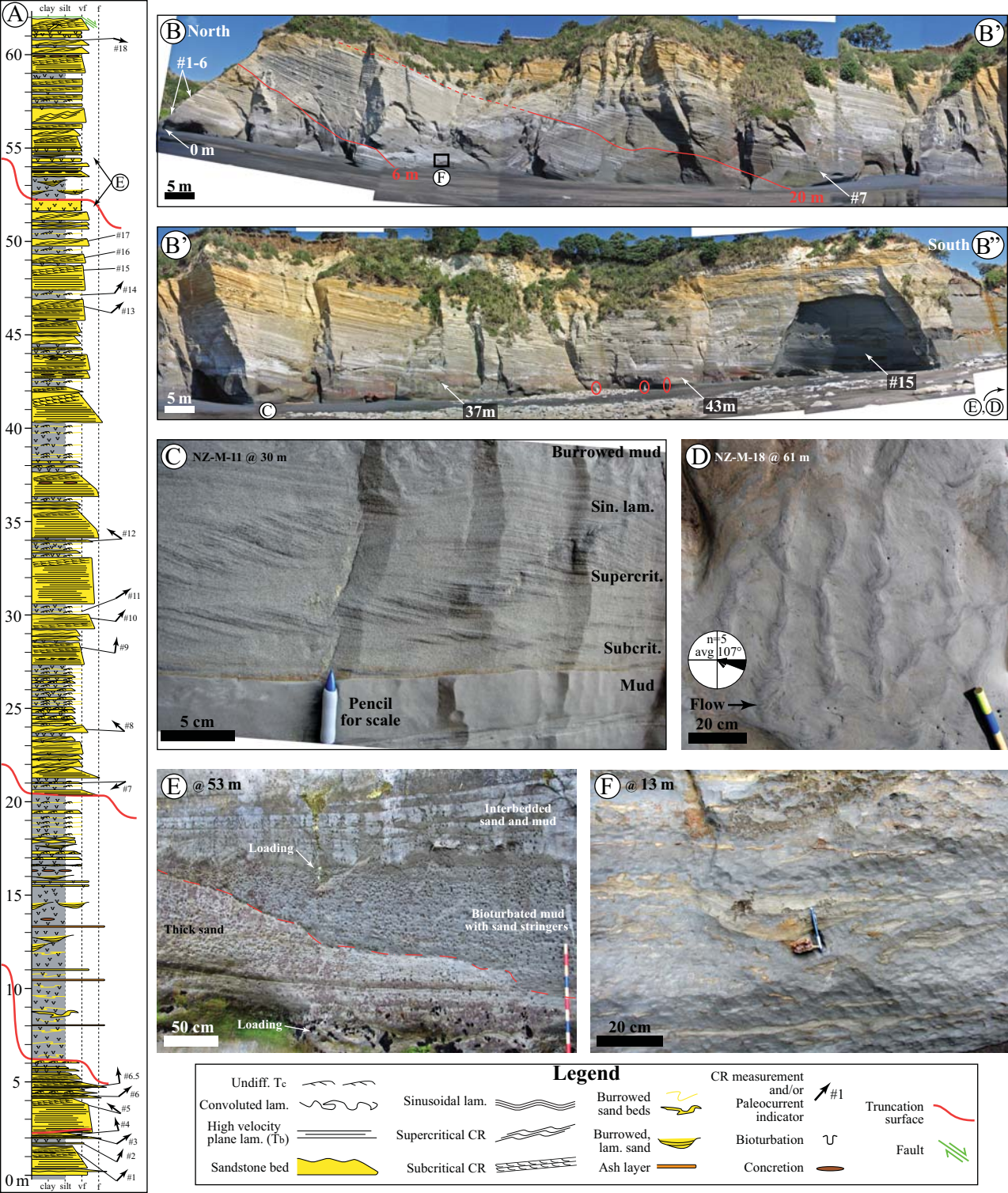


Figure 12. Characterization of the ZA locale.

(A) Map of the Kleine Reit Fontein locale, showing Fan 3 outcrop trend in yellow and measured section locations in red. White arrows indicate average paleocurrent directions for each section while all paleocurrents are plotted at right; see Fig. 4D for regional paleoflow information. Note the location of the cross section (D).

(B) Oblique plan view of the complex, three-dimensional sinuous and linguoid CRs common in the ZA locale. Pen for scale.

(C) Small-scale scour in the Kleine Ret Fontein area, marked by dashed red line. Typically, the scour topography is infilled rapidly by Facies 1. Geologist for scale; Jacob staff divisions are 10 cm.

(D) Depositional strike-oriented correlation panel of the Kleine Reit Fontein area; see (A) for location. Scour depth, width, and frequency all increase to the east and indicate increasing shear stress, possibly due to flow compression caused by intra-basinal topography present to the west (see text). For legend, see Figure 11.

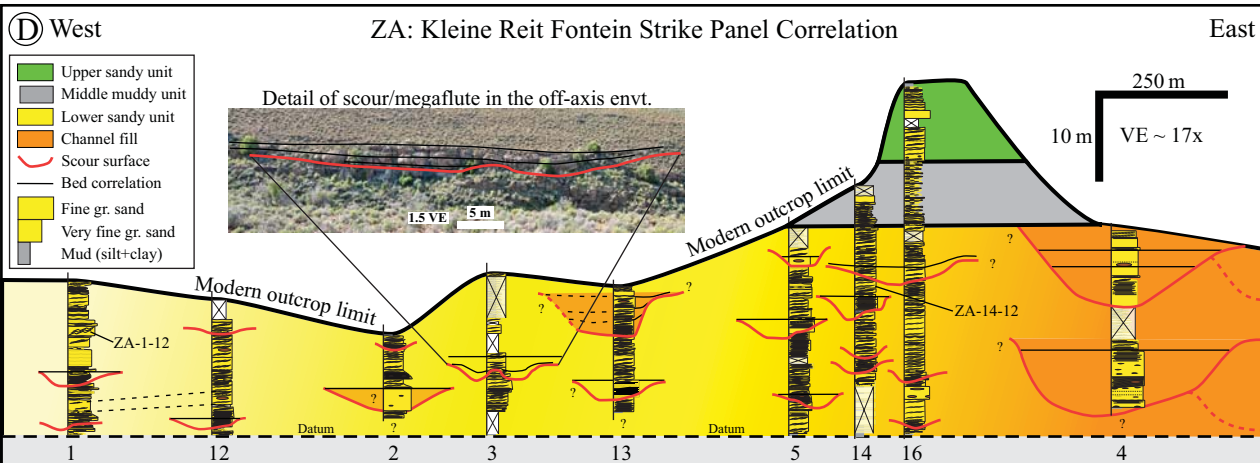
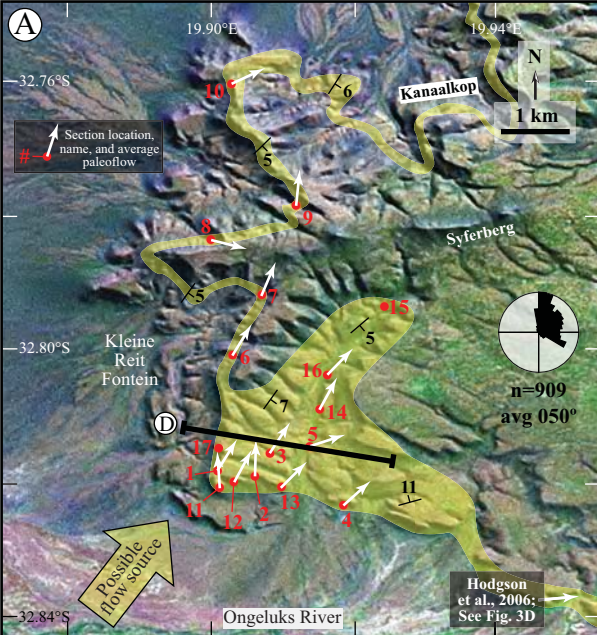


Figure 13. Characterization of the MAG locale.

(A) Map of the southern Titan mini-basin, with oil fields in green. Red lines indicate well bore penetrations of the Magnolia Field and the wells shown in C and D are highlighted in blue.

Dashed box indicates the location of (B). Numbers indicate Garden Banks block numbers.

(B) Structure map of the top main reservoir overlain with the RMS amplitude of the entire main reservoir interval (high amplitude values are red, low values are blue). Note that amplitudes in Magnolia indicate fluid phase rather than lithology; depositional elements are difficult to characterize using amplitude. The main reservoir thins southward onto the salt high. Faults drawn in red and generally dip to the north. Selected wells shown in green; 2ST2 is the cored well shown in (C) and A7 is the axial well, shown in (D).

(C) Dip seismic reflection profile through Magnolia field; main reservoir interval highlighted in yellow. The cored 2ST2 well displays heterogenous log response. Note the extensive faulting (red lines) and chaotic reflections, especially in updip locations.

(D) Strike seismic reflection profile through Magnolia near the A7 well, showing the chaotic nature of the main reservoir interval and the log response of the interpreted axial environment.

(E) The core of the main reservoir interval from the 2ST2 well, composed primarily of CRCL and scour fill deposits. Note the extensive slumping and faulting of the upper part of the main reservoir interval. For legend, see Figure 11.

(F) 4 feet (1.2 m) of typical CRCL deposits in Magnolia field. The presence of CRCL and flame structures suggest rapid deposition. Note the thick interbedded mudstones draping and preserving original ripple topography, indicating non-erosive flows.

(G) Soft sediment deformation and convoluted lamination/bedding of the cored interval, suggesting a topographically complex depositional environment due to salt movement.

(H) Faulting of the cored interval as a result of syn- and post-depositional salt movement. These faults have minor offsets but nonetheless create heterogeneity; many faults have larger offsets - see (E).

(I) Mud chip-lined scour and associated dip change observed in the cored interval. Note the slumped and convoluted bedding overlying the scour surface, suggesting depositional topography was created by the scour.

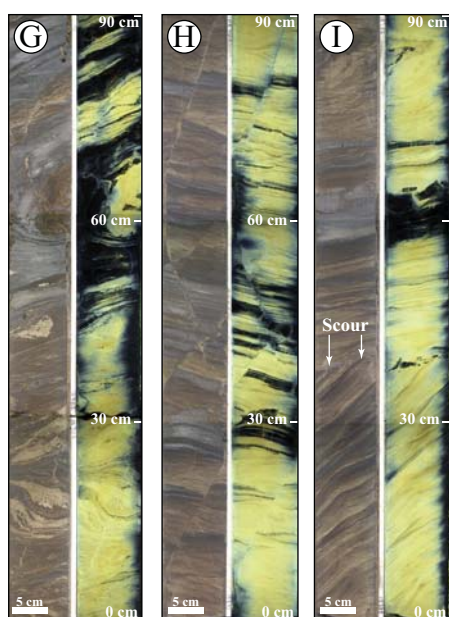
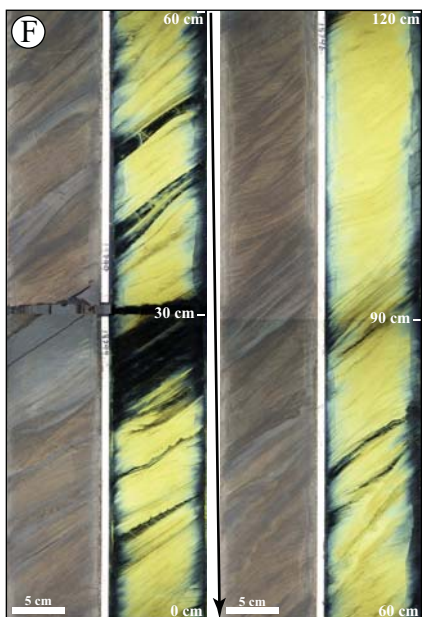
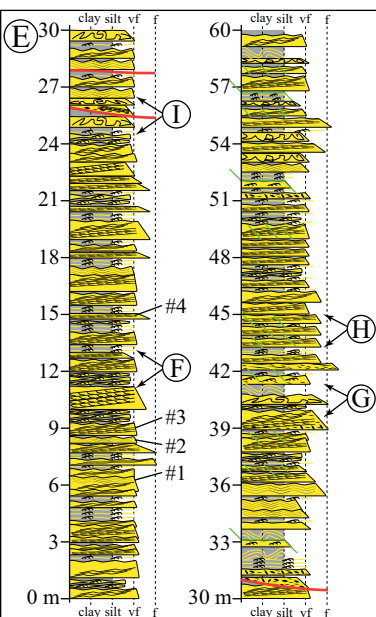
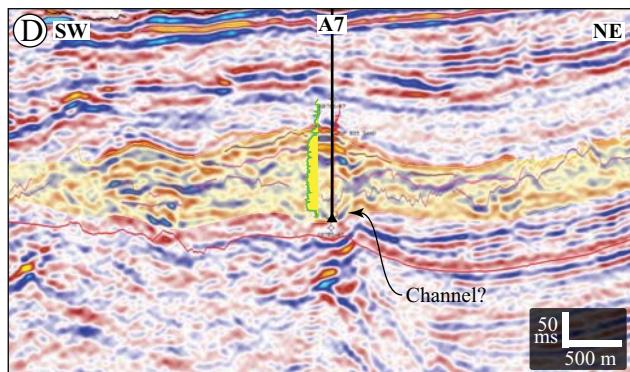
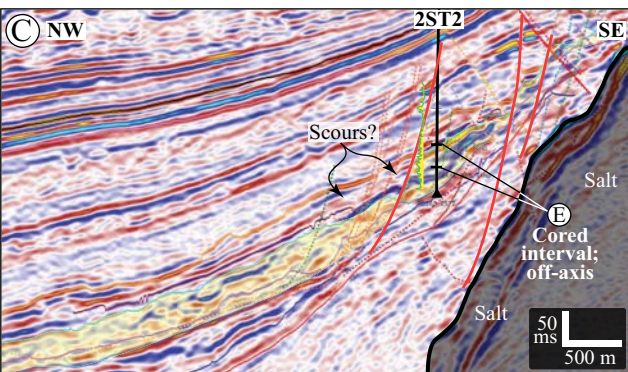
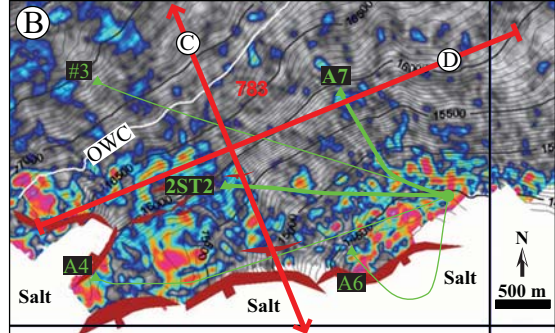
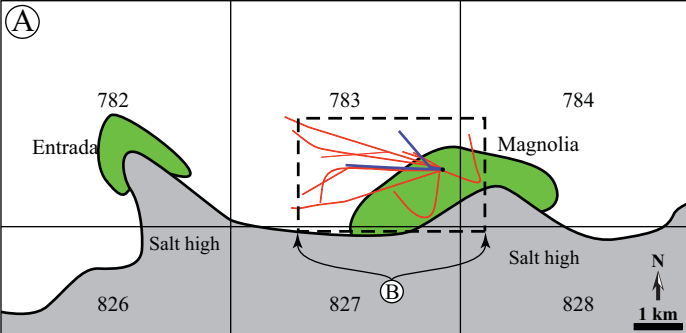


Figure 14. Schematic diagrams of the CRCL-promoting depositional environments in the three studied locales.

(A) The NZ locale, showing its location at the base of slope in a channelized environment; therefore, channels would be experiencing a gradient decrease. Inset box shows a potential channel near this change in gradient, resulting in intra-channel CRCL deposition as well as overbank CRCL deposition due to flow stripping. If a slump on either margin locally widened the channel, flows may expand in these zones, creating CRCL deposition inside the channel as well. Likely, the combination of these factors explains the presence of intra-channel CRCL formation in the NZ locale.

(B) The ZA locale may have had multiple flow sources: 1) a basin entry point to the southwest, and 2) a hypothetical western channel that supplied flow-stripped turbidity currents to the ZA locale. CRCL was formed due to flow expansion, but as flows neared the inferred topographic buttress, they eroded progressively larger scours, finally resulting in axial channel formation.

(C) The MAG locale, where decreasing gradient near the basin sill caused channelized flows to expand and thin, resulting in CRCL deposition. Channelization and scour intensity decrease with loss of channelization, with only small scours seen in the 2ST2 well. However, scour intensity may increase as flows become focused by the sill topography. After reaching the top of the sill, the remainder of the flow likely continued downslope, re-invigorated by the increased gradient.

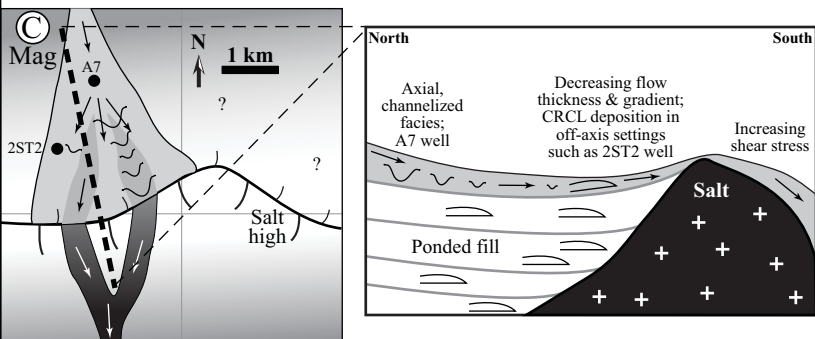
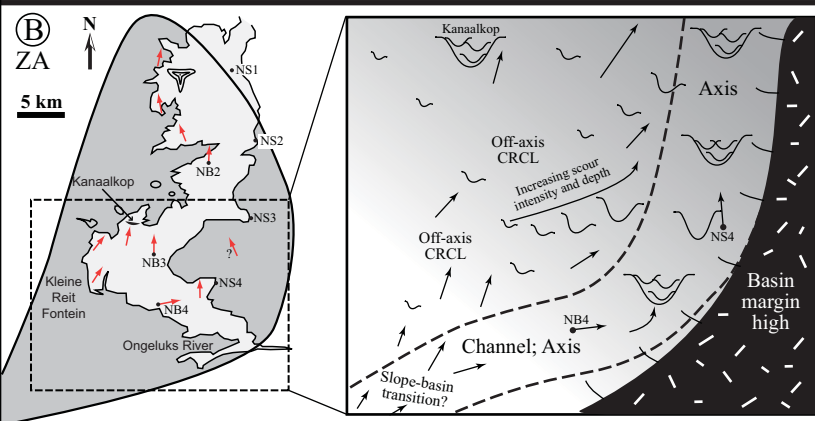
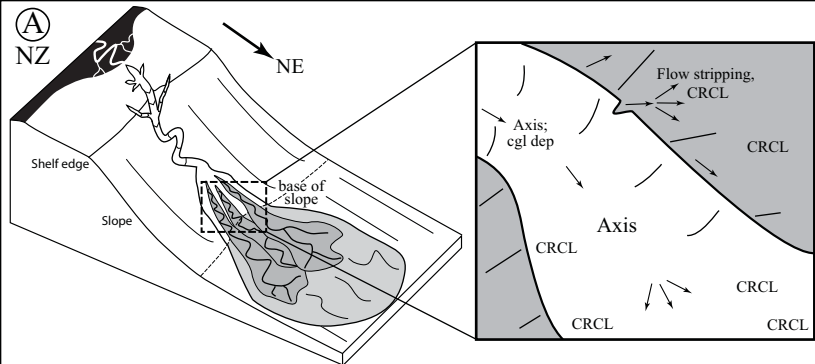


Figure 15. Diagrammatic representation of CRCL deposits and the variables of the TDURE model (modified from Baas et al., 2000; Baas, 2004). H_{bc} and H_{cd} are the ripple heights at the T_{bc} and T_{cd} boundaries, respectively, and λ is the ripple wavelength. X is the total horizontal displacement of a ripple train and z_c is the thickness of the T_c division. The ripple climb angle ζ (zeta) can be split into two vectors, $\mathbf{R}(t)$, the sedimentation rate and $\mathbf{u}_r(t)$, the ripple migration rate at time t . \mathbf{R}_{ab} , \mathbf{R}_{bc} , \mathbf{R}_{cd} are the sedimentation rates at turbidite divisions z_{ab} , z_{bc} , and z_{cd} . θ'_{bc} and θ'_{cd} are the grain-related mobility parameters at the noted boundaries and θ'_{crit} is the parameter at which bedload transport ceases according to Shields.

Flow direction \longrightarrow

Sedimentation rate $R(t)$

Ripple migration rate $u_r(t)$

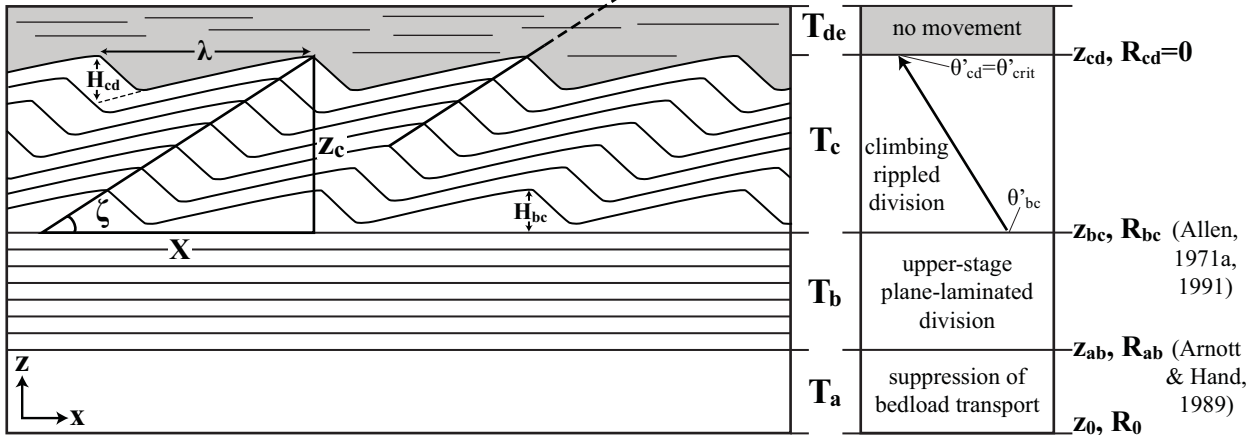


Figure 16. CRCL measurement frequency distributions. Frequency distribution of height H , wavelength λ , and climb angle ζ of CRCL deposits measured by this study; grain sizes vary from 84 to 149 μm . This study's ripple indices average 9.5. Colored arrows indicate average and equilibrium values for H , λ , and ζ from this and various other studies.

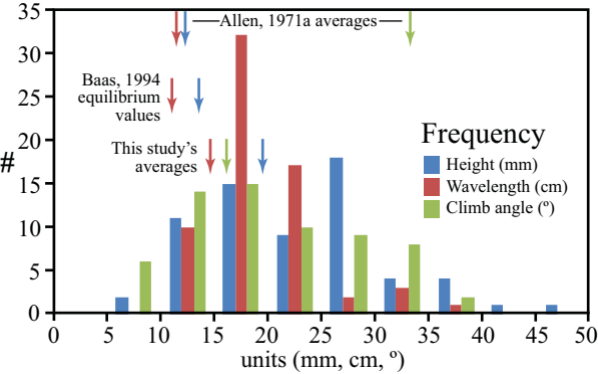


Figure 17. Plots of flow properties through the 44 sedimentation units from the NZ, ZA, and MAG locales.

(A) Plot of CRCL-only sedimentation rate R_{bc} (excluding T_a or T_b divisions) calculated by TDURE. Stratigraphic height increases from left to right for each locale. Average sedimentation rate for all locales is 0.15 mm/s. Note the increasing sedimentation rate throughout the NZ-M locale, indicating a gradual decrease in channel confinement through time.

(B) CRCL-only accumulation times τ_c calculated by TDURE. Note that most NZ beds fall in the 10-40 minute range, while a few Facies 1 beds are of much longer duration.

(C) Whole bed accumulation times (τ_{abc}). Note the contrast in flow durations between NZ locales, suggesting a change in depositional environment through time.

(D) Plot of climb angle ζ against observed height H – note the positive correlation, especially in NZ-M samples, the most densely sampled locale. This correlation indicates that the assumption of ripple height-sedimentation rate independence may not suffice for this dataset (see text).

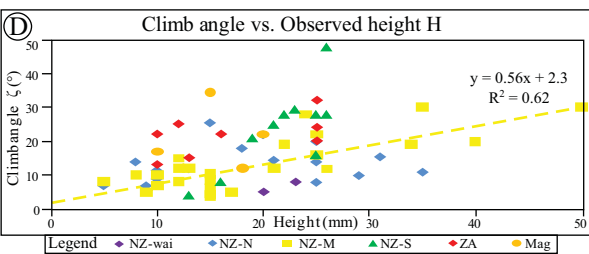
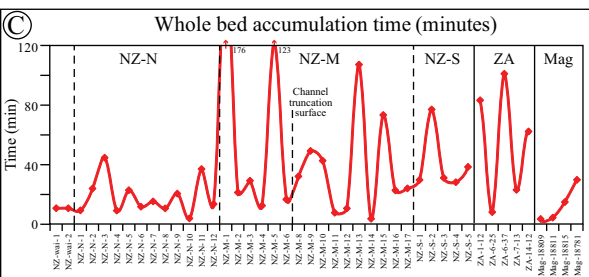
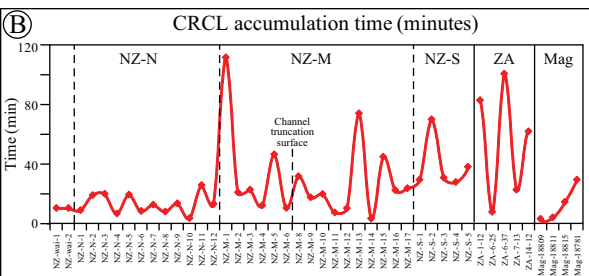
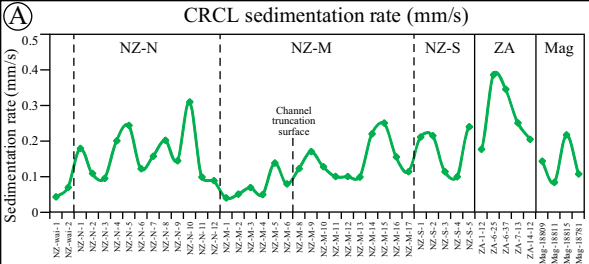
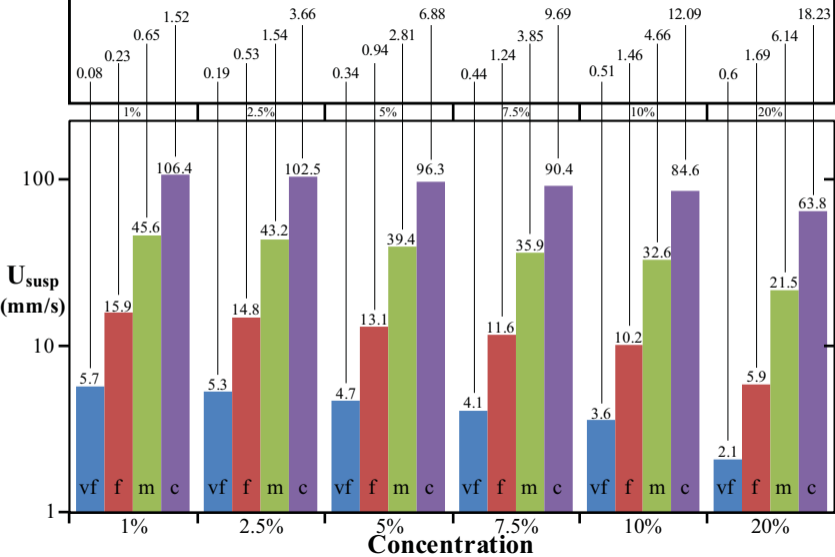


Figure 18. The effect of concentration on settling velocity and sedimentation rates of sediment suspensions. Very fine and fine sand settles in a viscous manner while coarse grained sand settles inertially; medium sand is transitional. Thus, U_{susp} , the hindered settling velocity, is more adversely affected for fine and very fine sand than for medium and coarse sand. For fine grained systems, low U_{susp} at concentrations less than 10% allows for the formation of CRCL by providing a sedimentation rate U_{bed} of approximately 0.2 mm/s. For coarse grained systems at similar concentrations, U_{bed} is above the 0.67 mm/s bedload suppression rate R_{ab} , resulting in formation of $T_a/S3$ divisions.

Sedimentation rate U_{bed} in mm/s



REFERENCES

- Adeogba, A.A., McHargue, T.R. and Graham, S.A., 2005, Transient fan architecture and depositional controls from near-surface 3-D seismic data, Niger Delta continental slope. *American Association of Petroleum Geologists, Bulletin*, v. 89, p. 627-643, doi:10.1306/11200404025
- Allen, J.R.L., 1963, Asymmetrical ripple marks and the origin of water-laid cosets of cross-strata. *Liverpool Manchester Geological Journal*, v. 3, no. 2, pp. 187-236, doi:10.1002/gj.3350030201
- Allen, J.R.L., 1968, *Current Ripples*, North-Holland, Amsterdam, 433 p.
- Allen, J.R.L., 1970, A quantitative model of climbing ripples and their cross-laminated deposits. *Sedimentology* v. 14, p. 5-26.
- Allen, J.R.L., 1971a, A Theoretical and Experimental Study of Climbing-Ripple Cross-Lamination, with a Field Application to the Uppsala Esker. *Geografiska annaler [1651-3215]* vol 53, pg 157-187.
- Allen, J.R.L., 1971b, Instantaneous sediment deposition rates deduced from climbing-ripple cross-lamination. *Journal of the Geological Society of London*, v. 127, p. 553-561.
- Allen, J.R.L., 1973, A classification of climbing-ripple cross-lamination. *Journal of the Geological Society of London*, v. 129, p. 537-541.
- Allen, J.R.L., and Leeder, M.R., 1980, Criteria for the instability of upper-stage plane beds. *Sedimentology*, v. 27, no. 2, p. 209-217, doi:10.1111/j.1365-3091.1980.tb01171.x
- Allen, J.R.L., 1991, The Bouma Division A and the Possible Duration of Turbidity Currents. *Journal of Sedimentary Petrology*, v. 61, p. 291-295.
- Amy, L.A., and Talling, P.J., 2006, Anatomy of turbidites and linked debrites based on long distance (120 x 30 km) bed correlation, Marnoso Arenacea Formation, Northern Apennines, Italy. *Sedimentology*, v. 53, no. 1, p. 161-212, doi:10.1111/j.1365-3091.2005.00756.x
- Armitage, D.A., Romans, B.W., Covault, J.A., and Graham, S.A., 2009, The Influence of Mass-Transport-Deposit Surface Topography on the Evolution of Turbidite Architecture: The Sierra Contreras, Tres Pasos Formation (Cretaceous), Southern Chile. *Journal of Sedimentary Research*, v. 79, no. 5, p. 287-301, doi:10.2110/jsr.2009.035
- Arnott, R.W.C. and Hand, B.M., 1989, Bedforms, primary structures and grain fabric in the presence of sediment rain. *Journal of Sedimentary Research*, v. 59, no. 6, p. 1062-1069.
- Ashley, G.M., Southard, J.B., and Boothroyd, J.C., 1982, Deposition of climbing-ripple beds: a flume simulation. *Sedimentology*, v. 29, p. 67-79.
- Baas, J.H., 1994, A flume study on the development and equilibrium morphology of current ripples in very fine sand. *Sedimentology*, v. 41, p. 185-209.
- Baas, J.H., 1999, An empirical model for the development and equilibrium morphology of current ripples in fine sand. *Sedimentology*, v. 46, p. 123-138.
- Baas, J.H., Van Dam, R.L., Storms, J.E.A., 2000. Duration of deposition from decelerating high-density turbidity currents. *Sedimentary Geology*, v. 136, p. 71-88, doi:10.1016/S0037-0738(00)00088-9
- Baas, J.H., 2004, Conditions for formation of massive turbiditic sandstones by primary depositional processes. *Sedimentary Geology*, v. 166, no. 3-4, p. 293-310, doi:10.1016/j.sedgeo.2004.01.011
- Bagnold, R.A., 1966, An approach to the sediment transport problems from general physics. U.S.G.S. Professional Paper 422-I.
- Bouma, A.H., 1962, *Sedimentology of some flysch deposits: a graphic approach to facies interpretation*. Amsterdam, Elsevier, 168 p.
- Bridge, J.S., 1997, Thickness of sets of cross strata and planar strata as a function of formative bed-wave geometry and migration and aggradation rate. *Geology*, v. 25, p. 971-974.
- Browne, G.H., Slatt, R.M., and King, P.R., 2000, Contrasting styles of basin-floor fan and slope fan deposition: Mount Messenger Formation, New Zealand, *in* A.H. Bouma and C.G. Stone, eds., *Fine-grained turbidite systems*. AAPG Memoir 72/SEPM Special Publication 68, p. 143-152.
- Browne, G.H. and R.M. Slatt, 2002, Outcrop and Behind-Outcrop Characterization of a Late Miocene Slope Fan System, Mt. Messenger Formation, New Zealand. *AAPG Bulletin*, v. 86, p. 841-862.
- Bucher, W.H., 1919, On ripples and related sedimentary surface forms and their paleogeographic interpretation. *American Journal of Sciences*, v. 47, p. 149-210, 241-269.
- Bursik, M.I. and Woods, A.W., 2000, The effects of topography on sedimentation from particle-laden turbulent density currents. *Journal of Sedimentary Research*, v. 70, p. 53-63.
- Clark, I.R., and Cartwright, J.A., 2009, Interactions between submarine channel systems and deformation

- in deepwater fold belts: Examples from the Levant Basin, Eastern Mediterranean sea. *Marine and Petroleum Geology*, v. 26, no. 8, p. 1465-1482, doi:10.1016/j.marpetgeo.2009.05.004
- Doyle, J.D., and Sweet, M.L., 1995, Three-Dimensional Distribution of Lithofacies, Bounding Surfaces, Porosity, and Permeability in a Fluvial Sandstone--Gypsy Sandstone of Northern Oklahoma. *American Association of Petroleum Geologists, Bulletin*, v. 79, no. 1, p. 70-96.
- Dreyer, T. Scheie, A., and Walderhaug, O., 1990, Minipermeameter-Based Study of Permeability Trends in Channel Sand Bodies. *American Association of Petroleum Geologists, Bulletin*, v. 74, no. 4, p. 359-374.
- Elliott, T., 2000, Megaflute erosion surfaces and the initiation of turbidite channels. *Geology*, v. 28, no. 2, p. 119-122, doi:10.1130/0091-7613(2000)28<119:MESATI>2.0.CO;2
- Fildani, A., Normark, W.R., Kostic, S. and Parker, G. 2006, Channel formation by flow stripping: large-scale scour features along the Monterey East Channel and their relation to sediment waves. *Sedimentology*, v. 53, p. 1265-1287.
- Fildani, A., N.J. Drinkwater, A. Weislogel, T. McHargue, D.M. Hodgson, and S.S. Flint, 2007, Age controls on the Tanqua and Laingsburg deep-water systems: new insights on the evolution and sedimentary fill of the Karoo basin, South Africa. *Journal of Sedimentary Research*, v. 77, p. 901-908.
- Haddad, G., Petersen, M., Waszczak, R.F., Young, S.W., Hufnagel, J.V., Liu, C.J., Palmer, J.R., Chlumsky, F.J., Borbas, T., Moutoux, J.J., McGee, D.T., Fitzsimmons, R.F., and Travis, P.D., 2003, Stratigraphic Evolution of the Magnolia Field and Surrounding Area, Garden Banks Blocks 783 and 784, Deepwater Gulf of Mexico. 2003 AAPG Annual Meeting Abstracts.
- Harms, J.C., Southard, J.B., Spearing, D.R., and Walker, R.G., 1975, Depositional Environments as Interpreted from Primary Sedimentary Structures and Stratification Sequences. Lecture notes, SEPM short course 2.
- Hedberg, H.D., 1926, The Effect of Gravitational Compaction on the Structure of Sedimentary Rocks. *American Association of Petroleum Geologists Bulletin*, v. 10, p. 1035-1072, doi:10.1306/3D932750-16B1-11D7-8645000102C1865D
- Heezen, B.C and Ewing, W.M, 1952, Turbidity currents and submarine slumps, and the 1929 Grand Banks [Newfoundland] earthquake. *American Journal of Science*, v. 250, p. 849-873.
- Hiscott, R.N., 1994, Loss of capacity, not competence, as the fundamental process governing deposition from turbidity currents. *Journal of Sedimentary Research*, v. 64, no. 2a, p. 209-214.
- Hodgson D.M., Flint S.S., Hodgetts D., Drinkwater N.J., Johannessen E.P. & Luthi S.M., 2006, Stratigraphic evolution of fine-grained submarine fan systems, Tangua Depocentre, Karoo Basin, South Africa. *Journal of Sedimentary Research*, v. 76, p. 19-39.
- Hunter, R.E., 1977, Terminology of Cross-Stratified Sedimentary Layers and Climbing-Ripple Structures. *Journal of Sedimentary Research*, v. 47, p. 697-706.
- Jobe, Z.R., Morris, W.R., Wickens, H. deV., and Lowe, D.R., 2008, Thick successions of climbing-ripple and scour-fill deposits in overbank/off-axis deep-water environments: Tanqua Karoo, South Africa and Magnolia field, Gulf of Mexico, AAPG Technical Program, Annual Convention, San Antonio 2008.
- Jobe, Z.R., Bernhardt, A., Lowe, D.R., 2010, Facies and architectural asymmetry in a conglomerate-rich submarine channel fill, Cerro Toro Formation, Sierra del Toro, Magallanes Basin, Chile, *Journal of Sedimentary Research*, v. 80, no. 12, pp 1085-1108, doi:10.2110/jsr.2010.092
- Johnson, S.J., Flint, S.S., Hinds, D., and Wickens, H. deV., 2001a, Anatomy, geometry and sequence stratigraphy of basin floor to slope turbidite systems, Tanqua Karoo, South Africa. *Sedimentology*, v. 48, p. 987-1023.
- Johnson, K.S., Paull, C.K., Barry, J.P., and Chavez, F.P., 2001b, A decadal record of underflows from a coastal river into the deep sea. *Geology*, v. 29, no. 11, p. 1019-1022, doi:10.1130/0091-7613(2001)029<1019:ADROUF>2.0.CO;2
- Jopling, A.V. and Walker, R.G., 1968, Morphology and origin of ripple-drift cross-lamination, with examples from the Pleistocene of Massachusetts. *Journal of Sedimentary Research*, v. 38, no. 4, p. 971-984.
- Kane, I.A., McCaffrey, W.D., and Martinsen, O.J., 2009, Allogenic vs. Autogenic Controls on Megaflute Formation. *Journal of Sedimentary Research*, v. 79, no. 9, p. 643-651, doi: 10.2110/jsr.2009.072

- Kane, I.A., McGee, D.T., and Jobe, Z.R., in press, Active salt controls on submarine channel evolution, and implications for facies architecture: Magnolia Field, Gulf of Mexico. Geological Society of London special publication: Salt Tectonics, Sediments and Prospectivity
- King, P.R., and Trasher, G.P., 1992, Post-Eocene development of the Taranaki Basin, New Zealand, convergent overprint of a passive margin, *in* J.S. Watkins, F. Zhiqiang, and K.J. McMillen, eds., *Geology and geophysics of continental margins*. AAPG Memoir 53, p. 93-118.
- King, P.R., Scott, G.H., and Robinson, P.H., 1993, Description, correlation and depositional history of Miocene sediments outcropping along the North Taranaki coast. Institute of Geological and Nuclear Sciences Monograph 5, 145 p.
- King, P.R., Browne, G.H., and Slatt, R.M., 1994, Sequence architecture of exposed late Miocene basin floor fan and channel-levee complexes (Mount Messenger Formation), Taranaki Basin, New Zealand, *in* P. Weimer, A.H. Bouma, and B.F. Perkins, eds., *Submarine fans and turbidite systems*. Gulf Coast Section SEPM 15th Annual Research Conference, p. 177-192.
- King, P.R., and Thrasher, G.P., 1996, Cretaceous-Cenozoic geology and petroleum systems of the Taranaki Basin, New Zealand. Institute of Geological and Nuclear Sciences Monograph 13, 243 p.
- King, P.R., 2000, Tectonic reconstruction of New Zealand: 40 Ma to Present. *New Zealand Journal of Geology and Geophysics* 43 (2000), pp. 611-638.
- Kneller, B., 1995, Beyond the turbidite paradigm: physical models for deposition of turbidites and their implications for reservoir prediction. *Geological Society of London Special Publications* 94, p. 31-49.
- Kuenen, Ph.H., 1953, Significant features of graded bedding. *Association of Petroleum Geologists, Bulletin*, v. 37, no. 5, p. 1044-1066.
- Kuenen, Ph.H., 1967, Emplacement of flysch-type sand beds. *Sedimentology*, v. 9, no. 3, p. 203-243, doi:10.1111/j.1365-3091.1967.tb02039.x
- Lamb, M.P., Toniolo, H., and Parker, G., 2006, Trapping of sustained turbidity currents by intraslope minibasins. *Sedimentology*, v. 53, p. 147-160.
- Leeder, M., 1999 *Sedimentology and sedimentary basins: from turbulence to tectonics*. Blackwell Scientific Publications, Oxford, UK, 592 pp.
- Lowe, D.R., 1982, Sediment gravity flows: II. Depositional models with special reference to the deposits of high-density turbidity currents. *Journal of Sedimentary Petrology*, v. 52, no. 1, p. 279-297, doi:10.1306/212F7F31-2B24-11D7-8648000102C1865D
- Luthi, S.M., Hodgson, D.M., Geel, C.R., Flint, S.S., Goedbloed, J.W., Drinkwater, N.J. and Johannessen, E.P., 2006, Contribution of research borehole data to modelling fine-grained turbidite reservoir analogues, Permian Tanqua-Karoo basin-floor fans (South Africa). *Petroleum Geoscience*, v. 12, no. 2, p. 175-190, doi:10.1144/1354-079305-693
- Maier, K.L., Fildani, A., Paull, C.K., Graham, S.A., McHargue, T., Graham, S.A., Caress, D.W., McGann, M.M., 2011, The elusive character of discontinuous deep-water channels: New insights from Lucia Chica channel system, offshore California. *Geology*, vol. 39, no. 4, pp. 327-330.
- Maude, A.D., and Whitmore, R.J., 1958, A generalized theory of sedimentation. *British Journal of Applied Physics*, v. 9, p. 477-482, doi:10.1088/0508-3443/9/12/304
- McCarthy, P., Brand, J., Paradiso, B., Ezekwe, J., Wiltgen, N., Bridge, A., Willingham, R., and Bogaards, M., 2005, Using geostatistical inversion of seismic and borehole data to generate reservoir models for flow simulations of Magnolia Field, deepwater Gulf of Mexico. *SEG Expanded abstracts*, v. 24, p. 1351.
- McCarthy, P., Brand, J., Paradiso, B., Ezekwe, J., Wiltgen, N., Bridge, A., Willingham, R., and Bogaards, M., 2006, Using geostatistical inversion of seismic and borehole data to generate reservoir models for flow simulations of Magnolia Field, deepwater Gulf of Mexico. *Sixth International Conference and Exposition on Petroleum Geophysics*, p. 573-576.
- McGee, D.T., Fitzsimmons, R.F., and Haddad, G.A., 2003, From Fill to Spill: Partially Confined Depositional Systems, Magnolia Field, Garden Banks, Gulf of Mexico. 2003 AAPG Annual Meeting Abstracts.
- McKee, E.D., 1966, Significance of climbing-ripple structure. U.S.G.S. Prof. Paper 550-D, p. D94-D103.

- Morris, W.R., Scheihing, M.H., Wickens, D.V. and Bouma, A.H., 2000 Reservoir architecture of deep-water sandstones from the Skoorsteenberg Formation, Tanqua Karoo Sub-Basin, South Africa, *in* P. Weimer, R.M. Slatt, J. Coleman, N.C. Rosen, H. Nelson, A.H. Bouma, M.J. Styzen, and D.T. Lawrence, eds., Deep-water reservoirs of the world. Gulf Coast Section, SEPM 20th Annual Research Conference, p. 629–649.
- Mutti, E., 1977, Distinctive thin-bedded turbidite facies and related depositional environments in the Eocene Hecho Group (South-central Pyrenees, Spain). *Sedimentology*, v. 24, p. 107-131.
- Mutti, E., and Normark, W.R., 1987, Comparing examples of modern and ancient turbidite systems: problems and concepts, *in* J.K. Leggett and G.G. Zuffa, eds., *Marine clastic sedimentology: concepts and case studies*. London, Graham and Trotman, p. 1-38.
- Normark, W.R., Piper, D.J.W., and Hess, G.R., 1979, Distributary channels, sand lobes, and mesotopography of Navy Submarine Fan, California Borderland, with applications to ancient fan sediments. *Sedimentology*, v. 26, no. 6, p. 749-774, doi: 10.1111/j.1365-3091.1979.tb00971.x
- Piper, D.J.W., and Normark, W.R., 1983, Turbidite depositional patterns and flow characteristics, Navy submarine fan, California borderland: *Sedimentology*, v. 30, p. 681-694.
- Pirmez, C., and Imran, J., 2003, Reconstruction of turbidity currents in Amazon Channel. *Marine and Petroleum Geology*, v. 20, p. 823–849, doi:10.1016/j.marpetgeo.2003.03.005
- Prather, B.E., Booth, J.R., Steffens, G.S., and Craig, P.A., 1998, Classification, lithologic calibration, and stratigraphic succession of seismic facies of intraslope basins, deep-water Gulf of Mexico. *American Association of Petroleum Geologists, Bulletin*, v. 82, p. 701-728.
- Prelat, A., Hodgson, D.M., and Flint, S.S., 2009, Evolution, architecture and hierarchy of distributary deep-water deposits: a high-resolution outcrop investigation from the Permian Karoo Basin, South Africa. *Sedimentology*, v. 56, no. 7, p. 2132-2154, doi:10.1111/j.1365-3091.2009.01073.x
- Prior, D.B., Bornhold, B.D., Wiseman, W.J., Jr and Lowe, D.R., 1987, Turbidity current activity in a British Columbia fjord. *Science*, v. 237, no. 4820, p. 1330-1333, doi:10.1126/science.237.4820.1330
- Pyles, D.R., 2008, Multiscale stratigraphic analysis of a structurally confined submarine fan: Carboniferous Ross Sandstone, Ireland. *American Association of Petroleum Geologists Bulletin*, v. 92, no. 5, p. 557-587, doi:10.1306/01110807042
- Raudkivi, A.J., 1963, A study of sediment ripple formation. *Journal of Hydraulic Engineering, ASCE*, v. 89, p. 15-33.
- Reineck, H.E., 1961, Sedimentbewegungen an Kleinrippeln im Watt. *Senckenbergiana Lethaea*, v. 42, p. 51-67.
- Reynolds, O., 1883, An experimental investigation of the circumstances which determine whether the motion of water shall be direct or sinuous, and of the law of resistance in parallel channels. *Philosophical Transactions of the Royal Society* v. 174, p. 935-982, doi:10.1098/rstl.1883.0029
- Richardson, J.F. and Zaki, W.N., 1954, Sedimentation and fluidisation: part 1. *Trans. Inst. Chem. Eng.* v. 32, p. 35–53.
- Rubin, D.M. and Hunter, R.E., 1982, Bedform climbing in theory and nature. *Sedimentology*, v. 29, p. 121-138.
- Sorby, H.C., 1852, On the oscillation of the currents drifting the sandstone beds of the southeast of Northumberland, and on the general direction in the coalfield in the neighbourhood of Edinburgh. *Proceedings of the Yorkshire Geological Society*, v. 3, p. 112-122.
- Sorby, H.C., 1859, On the structures produced by the currents present during the deposition of stratified rocks. *Geologist*, v. 2, p. 137-147.
- Southard, J.B., and Boguchwal, L.A., 1990, Bed configurations in steady unidirectional water flows, Part 2: Synthesis of flume data. *Journal of Sedimentary Research*, v. 60, no. 5, p. 658-679.
- Spain, D.R., 1992, Petrophysical Evaluation of a Slope Fan/Basin-Floor Fan Complex: Cherry Canyon Formation, Ward County, Texas. *Association of Petroleum Geologists, Bulletin*, v. 76, no. 6, p. 805-827.
- Stanley, K.O., 1974, Morphology and Hydraulic Significance of Climbing Ripples with Superimposed Micro-Ripple-Drift Cross-lamination in Lower Quaternary Lake Silts, Nebraska. *Journal of Sedimentary Research*, v. 44, no. 2, p. 472-483.
- Sumner, E.J., Amy, L.A., and Talling, P.J., 2008, Deposit Structure and Processes of Sand Deposition from Decelerating Sediment Suspensions. *Journal of Sedimentary Research*, v. 78, no. 8, p. 529-547, doi:10.2110/jsr.2008.062

- Tanner, W.F., 1967, Ripple mark indices and their uses. *Sedimentology*, v. 9, no. 2, pp. 89-104, doi:10.1111/j.1365-3091.1967.tb01332.x
- van den Berg, J.H., and van Gelder, A., 1993, A new bedform stability diagram, with emphasis on the transition of ripples to plane bed in flows over fine sand and silt. *in*: Marzo, M., Puigdefabregas, C., eds., *Alluvial Sedimentation*. International Association of Sedimentologists Special Publication, vol. 17, pp. 11– 21.
- van der Werff, W. and Johnson, S., 2003, High resolution stratigraphic analysis of a turbidite system, Tanqua Karoo Basin, South Africa. *Marine and Petroleum Geology*, v. 20, p. 45-69.
- Walker, R.L., 1963, Distinctive types of ripple-drift cross-lamination: *Sedimentology*, v. 2, p. 173-188.
- Walker, R.G., 1965, The origin and significance of the internal sedimentary structures of turbidites. *Proceedings of the Yorkshire Geological Society*, v. 35, p. 1–32.
- Walker, R.L., 1967, Turbidite sedimentary structures and their relationship to proximal and distal depositional environments: *Journal of Sedimentary Petrology*, v. 37 p. 25-43.
- Walker, R.G., 1969. Geometrical analysis of ripple-drift cross-lamination. *Canadian Journal of Earth Sciences*, v. 6, p. 383–391.
- Weissenburger, K.S., and Borbas, T., 2004, Fluid properties, phase and compartmentalization: Magnolia Field case study, Deepwater Gulf of Mexico, USA. *Geological Society of London, Special Publications* v. 237, p. 231-255, doi:10.1144/GSL.SP.2004.237.01.14
- Wickens, H.deV., 1994, Basin Floor Fan Building Turbidites of the Southwestern Karoo Basin, Permian Ecca Group, South Africa: Unpubl. Ph.D. thesis, University of Port Elizabeth, South Africa, 233 p.
- Wickens, H.deV. and Bouma, A.H. ,2000, The Tanqua fan complex, Karoo basin, South Africa: outcrop analog for fine-grained, deepwater deposits, *in* A.H. Bouma and J. Stone, eds., *Fine-Grained Turbidite Systems*. AAPG Memoir 72, p. 153-164.
- Wynn, R.B., Kenyon, N.H., Masson, D.G., Stow, D.A.V., and Weaver, P.P.E., 2002, Characterization and recognition of deep-water channel-lobe transition zones. *American Association of Petroleum Geologists, Bulletin*, v. 86, p. 1441-1462.